Review article

Evolution of red ceramic pigments: from hazardous compounds to environmentally friendly alternatives

Rayehe Tavakolipour [a,*], **Yueming Li** [b], **Maryam Hosseini Zori** [c,*],
Maria Ines Basso Bernardi [d], **Kun Li** [e], **Aušra Čiuladienė** [f], **Eva Miguel** [g]

a Department of Materials Engineering, Naghshejahan Institute of Higher Education, Baharestan, Isfahan, Iran

b School of Materials Science and Engineering, Jingdezhen Ceramic University; Jingdezhen 333403, China

c Department of Inorganic Pigments and Glazes, Institute for Color Science and Technology (ICST), Iran Ministry of Science, Research and Technology, PO Box: 1668814811, Tehran, Iran

d Sao Carlos Institute of Physics, University of Sao Paulo - USP, Sao Carlos - SP, Brazil

e School of Materials Science and Engineering, Shaanxi University of Technology, Hanzhong, Shaanxi, Postal code: 723001, Shaanxi, China

f The Wroblewski Library of the Lithuanian Academy of Sciences, Document Conservation and Restoration Department, Žygimantų str. 1, Vilnius, LT 01102, Lithuania

g Ceramic Technology Department, Escola Superior de Ceràmica de L'Alcora (ESCAL-ISEACV), 12110 L'Alcora, Spain

ABSTRACT

Synthesis of red ceramic pigments is a challenging task in the ceramic industry. Most classic reds are based on severely toxic materials including lead, arsenic, mercury, selenium, and cadmium, which are forbidden in many countries. On the other hand, the red color is super sensitive to the synthesis parameters, heat treatment conditions (atmosphere and temperature), particle size, etc. Therefore, achieving a bright true red shade and its stability at high temperatures is crucial. There has been a massive attempt to find a sustainable high-temperature resistant alternative for these hazardous compounds. Iron oxide is one of the first red pigments in history, but it cannot produce a bright red shade and its color is mostly red-brown. Ce_2S_3 is another red pigment with a beautiful red color. But it cannot stand the temperature above 350 °C in an oxidizing atmosphere. Doping lanthanides in the perovskites or entrapping the toxic beautiful chromophores in the core-shell structures are among the strategies to achieve safe bright red pigments. This review outlines the recent progress of hazardous classic reds to environmentally friendly ceramic red pigments. Various compounds and dopants, applied to develop sustainable reds, from simple iron-oxides to composites, solid solutions, core-shell structures, or even purified wastes have been covered in this review.

© 2024 The Authors. Published by Synsint Research Group.

OPEN ACCESS

1. Introduction

Color is a pervasive aspect of human life, contributing to the aesthetics of our daily environment [1]. As for every field of science aiming to protect the environment, developing new environmentally friendly nontoxic colored inorganic pigments is the ultimate goal of pigment science. Colored pigments are particulate coloring agents that are insoluble in the application system with an optical action based on selective light absorption and scattering [2]. Red, orange, and pink colored pigments have more limited applications due to their high atmospheric and thermal sensitivities, easy etching properties, and the presence of toxic elements in their structures [3]. Although some

fascinating properties have been obtained in the pigment systems containing Hg, Pd, Cr, Cd, Se, Sn, Sb, and As; their applications are restricted by the governments due to the toxicity for the environment and the human[4]. The current industrial red pigments are mainly based on these systems: $CdS-CdSe$, $Al_2O_3-Cr^{3+}$, $Zr.SiO_4-Fe^{3+}$, $MnAl_2O_4-Cr^{3+}$, $ZnAl_2O_4-Cr$, $Y_2Sn_{2-x}Cr_xO_{7-\delta}$, and $CaSnSiO_5-Cr^{3+}$ [5]. Lead molybdate and cadmium sulfoselenide are among the most famous red pigments with high opacity, UV resistance, and chemical and thermal stabilities, having wide applications in the ceramics, plastics, packaging, and automotive industries. However, their safety for humans and the environment is questionable [6]. Iron oxides and hydroxide pigments have been used from prehistoric (seen in cave paintings) and ancient eras up to now [2]. These pigments are environmentally friendly and economically beneficial. Hematite is a simple iron oxide with a red color and prolonged weather resistance, used as a red pigment for over 100,000 years. But hematite color is not pure vivid red it is red-brown [7]. Today, lanthanide oxides are replacing toxic elements such as lead, cobalt, chromium, and cadmium for developing stable new pigments [8] Cerium-based pigments have been increasingly produced and used lately, due to their nontoxic nature, high thermal and chemical stability, ultraviolet and infrared shielding, and good chromaticity. Additionally, encapsulation or inclusion of the unstable or toxic chromophore into a protective crystalline matrix is another strategy for developing high-performance red pigments [9, 10].

This review study aims to address the issues and challenges of red pigment synthesis that are required to be environmentally friendly, non-toxic, high-temperature resistant, lightfast, and chemical-proof. Satisfying all these requirements at the same time is a complicated task. At first, the CIELab color space as a determining factor of the pigment shades, saturation, and lightness is briefly introduced. Then, the red pigments are classified and discussed based on toxicity, structure, and composition.

2. CIELab color space

As the focus of this review is on color, it is crucial to briefly introduce the color interpretation method using one of the most applied techniques to investigate the chromaticity of the pigments, i.e. the CIELab color space. A typical color palette for a ceramic pigment is obtained using the a*-b* plane from the L*, b*, and a* coordinates (Fig. 1). +a*, -a*, +b*, and -b* show the red, green, yellow, and blue colors, respectively. The (+a*)-(+b*) plane covers warm colors, including red, orange, and yellows. The (-a*) and (-b*) parameters indicate the green to-blue colors, while (+b*)-(-a*) and (-b*)-(+a*) planes are related to the green-yellow and blue-purple color ranges, respectively. Meanwhile, L* and c* are lightness (100 for black and 0 for white) and chroma (▲: pure saturated color, ▼: pastel color) [11].

3. Classic red pigments

3.1. Minium

Minium (Pb_3O_4) is one of the oldest synthetic pigments with a bright red-orange color [12]. This pigment was confused with cinnabar, as it is named after the River Minius containing the cinnabar minerals [13]. It was extensively used in the manuscripts of the medieval period and that is why they were called "the miniatures". But its applications in the pigment industry have gradually decreased since the 20th century, due
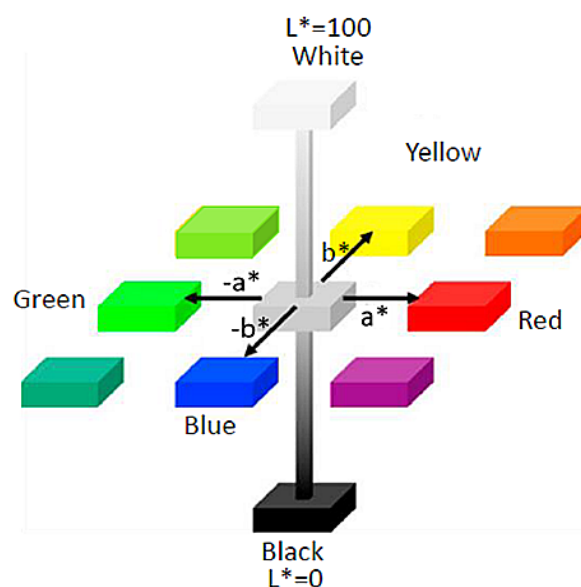

Fig. 1. The CIELab color space plot in three dimensions.

to lead toxicity [12]. The toxicity of lead relies on its acid solubility, releasing its metallic form in the stomach [13]. The minium history, synthesis method, and transformation products are reviewed elsewhere [14]. But it can be briefly mentioned that this pigment was accidentally obtained by roasting the lead white. The red lead pigments have whitening and blackening issues over time, mostly attributed to the effects of the impurities, the environmental conditions (light and humidity), CO_2, the binding media, the microorganisms, and chlorine salts. Lead is capable of accumulating in the body organs, including muscles, bones, kidneys, and the brain, leading to nervous, muscular, cardiovascular, and kidney malfunctions as well as decreasing the children's IQ. She et al. [15] reported the UV-assisted lead release from the semiconductor minium pigments in water, emphasizing their dangers for health and the environment. However, the minium pigments are still being used in developing countries due to the low production costs.

3.2. Cinnabar

Cinnabar (α-HgS) is a red pigment with many names in different cultures (e.g. šangarf in Persian or minium cinnabaris in Latin). The synthetic cinnabar was obtained by pulverizing scarlet-colored sand, collected from the Ephesus region, and its repeated washing by decanting. Cinnabar is unstable at above 315 °C and transforms into metacinnabar (β-HgS), changing its color from red to black [16]. Cinnabar has been applied as a pigment for thousands of years because this composition shows a deep red color with appropriate coverage and a unique gloss. The red color in most of the ancient objects is still there due to its resistance against acid rain or oxidation. This pigment could also be synthesized by a solid-state reaction between Hg and S elements. Then, the obtained HgS was converted to cinnabar through a sublimation process at 588 °C [17]. The properties and history of cinnabar have also been reviewed by various authors before [16, 17] and the reader is encouraged to seek for the comprehensive details over there.

3.3. Realgar

Realgar (α-As_4S_4) is a low-temperature soft (1/2 Mohs hardness) red pigment with a monoclinic structure. This pigment was recognized in the 18th century, but its crystallographic studies have begun since the 1950s [18]. Realgar was a common red pigment in ancient times until the early twentieth century [19]. The realgar has a covalently-bound cage-like structure, made of As-As and S-S dimers. There are two polymorphs for realgar, based on temperature: α- (low-temperature phase) and β-realgar (high-temperature phase). The α-realgar decomposes to pararealgar with a yellow-orange color upon air exposure [20, 21]. Arsenic is an abundant toxic carcinogenic element in the environment and its accumulation in the body results in severe diseases and even death. This element is considered the number one on the list of hazardous substances priority list in the USA. Cardiovascular disorders, bladder cancer, in-skin accumulations, oxidative stress, and type 2 diabetes are a few of the many consequences of prolonged exposure to arsenic [22]. 70% of realgar is constituted of arsenic. The released arsenic from this mineral has a higher mobility than the arsenic-containing iron sulfides. Because the divalent arsenic generates trivalent/pentavalent forms upon oxidation in the absence of iron these isotopes easily pollute groundwaters, soils, and rivers. Sunlight accelerates the arsenic release from realgar. Liu et al. [23] stated that the released arsenic percentage in the realgar solution increased from 4.2% (in darkness) to 18.1% under sunlight.

Čiuladienė et al. [19, 24] studied the historical red pigments including minium, realgar, cinnabar, red ochre, and red bolus in various binding media. SEM images of the pigments are shown in Fig. 2. Cinnabar had a platy morphology with a particle size of 2–5 μm, while the realgar particles were irregularly shaped with a wide particle size distribution (5–40 μm). Hematite, red lead, and the red ochre exhibited nanoscale spherical particles while the red bolus with a chemical composition of iron aluminum silicate had platy micro-sized pigments in a range of 1–10 μm. The digital images of the red-orange paints made of cinnabar, realgar, and red lead (minium) as well as the binding media (gum Arabic, fish glue, and parchment glue) before and after aging for 35 days are shown in Fig. 3 and the related chromaticity data are also represented in Table 1. ΔE is the color difference, calculated by Eq. 1:

$$\Delta E = \left[(\Delta L^*)^2 + (\Delta a^*)^2 + (\Delta b^*)^2 \right]^{1/2} \tag{1}$$

where ΔL^*, Δa^*, and Δb^* are the differences of lightness-darkness, redness-greenness, and yellowness-blueness between the aged and non-aged paints. Cinnabar showed a deep red with the lowest color change ($\Delta E \leq 3$) in various binding media, excluding the fish glue ($\Delta E = 6.9$). Minium gave a red-orange color with almost similar performances in different media. However, the red lead colors changed significantly after aging. Realgar showed the highest color change from red-orange to even greenish hues in the case of gum Arabic.

3.4. Molybdate red

Molybdate red is a solid-solution pigment with a tetragonal structure, consisting of $PbCrO_4$ and $PbMoO_4$. Inclusions of small amounts of $PbSO_4$ are also possible. The molybdate addition gives a bright orange-red color to the yellow lead chromate [25]. Schultze discovered the chemistry of the Molybdate red in 1863 by observing a bright red color in the wulfenite-conjugated crocoite. The production of this orange-red pigment dates back to almost a century ago. The lead chromate pigments have low resistance to the weather, light, SO_2, and
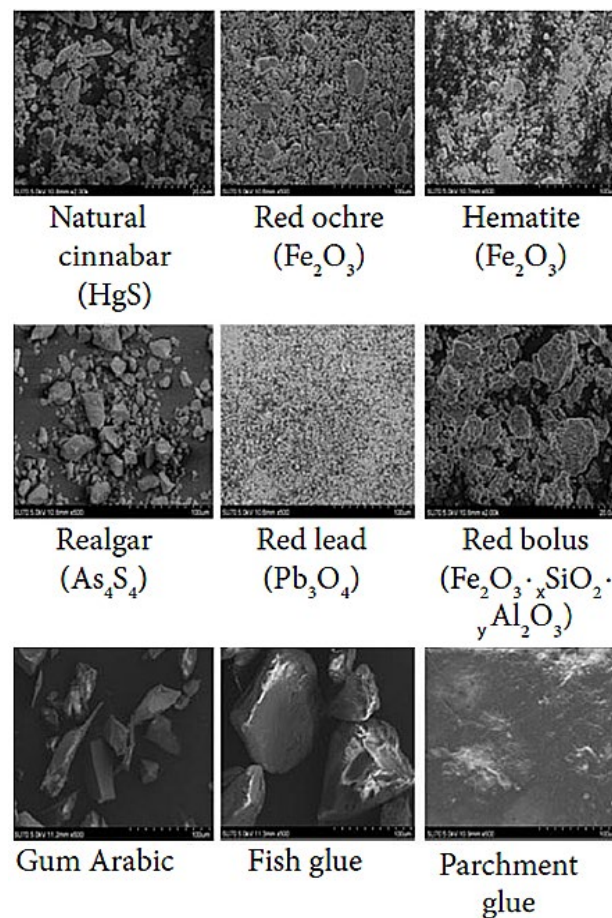
Fig. 2. SEM images of classic red pigments with the applied binding media. "Reproduced with permission from Ref. [24]".

acid/alkaline. So, they are often encapsulated in the oxides of antimony, titanium, silicon, and tin [26]. The Molybdate red is often produced using the Sherwin-Williams or the Bayer process. The Sherwin-Williams process involves a reaction between lead nitrate and a solution consisting of sulfuric acid, ammonium molybdate, and
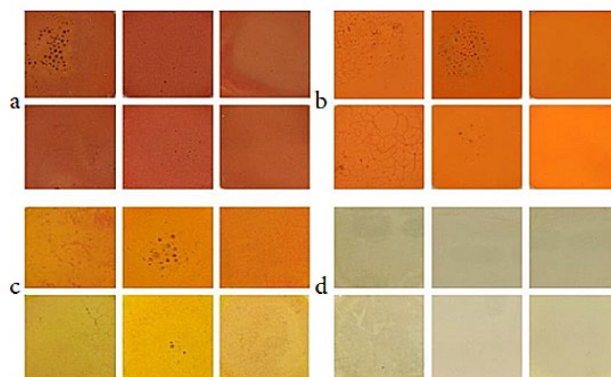
Fig. 3. Digital photos of a) cinnabar, b) red lead (minium), c) realgar, and d) (left to right) gum Arabic, fish glue, and parchment glue before (top) and after (bottom) aging for 35 days. "Reproduced with permission from Ref. [19]".

Table 1. The chromaticity values of the prepared red paints before and after aging for 35 days. "Reproduced with permission from Ref. [19]".

Pigment		Gum Arabic		Fish glue		Parchment glue	
		Before	After	Before	After	Before	After
Cinnabar	L*	52.6	50.7	56.1	53.2	65.9	65.1
	a*	37.8	36.2	42.2	38.5	39.8	38.7
	b*	31.5	30.5	32.8	27.7	32.9	31.5
	ΔE	-	2.7	-	6.9	-	2.0
Red lead	L*	70.9	69.3	67.8	65.6	78.1	72.9
	a*	51.1	48.8	50.5	47.3	54.2	49.3
	b*	54.3	56.7	54.9	57.6	61.1	56.5
	ΔE	-	3.7	-	4.7	-	7.7
Realgar	L*	7.6	75.4	72.9	73.5	75.5	83.7
	a*	42.9	16.1	40.7	20.9	43.6	15.9
	b*	57.8	43.3	62.8	59.7	55.4	25.5
	ΔE	-	30.4	-	20.0	-	41.5

Fig. 4. Crystal structure of the cadmium sulfoselenide red pigments. "Reproduced from Ref. [29] with permission from Elsevier. All rights reserved".

sodium di-chromate, while the Bayer process is based on sodium sulfate, potassium di-chromate, ammonium molybdate, and lead nitrate. Molybdate red provides good coverage with brilliant hues [2]. Large amounts of chromium and lead in the Molybdate red have brought environmental and health issues. In addition to the mentioned lead issues, chromium, as a carcinogenic material, can intensively affect the immune system, lungs, and skin. In a study [25], it was confirmed that the molybdenum accelerated the photo-dissolution of the Molybdate red under sunlight and increased the environmental risks compared to the lead chromate yellow. Molybdate red pigment, as a member of the lead chromates and molybdates group, is classified as a chronically toxic material. Although it is banned from the food consumer industries, it is still being applied in industrial coatings.
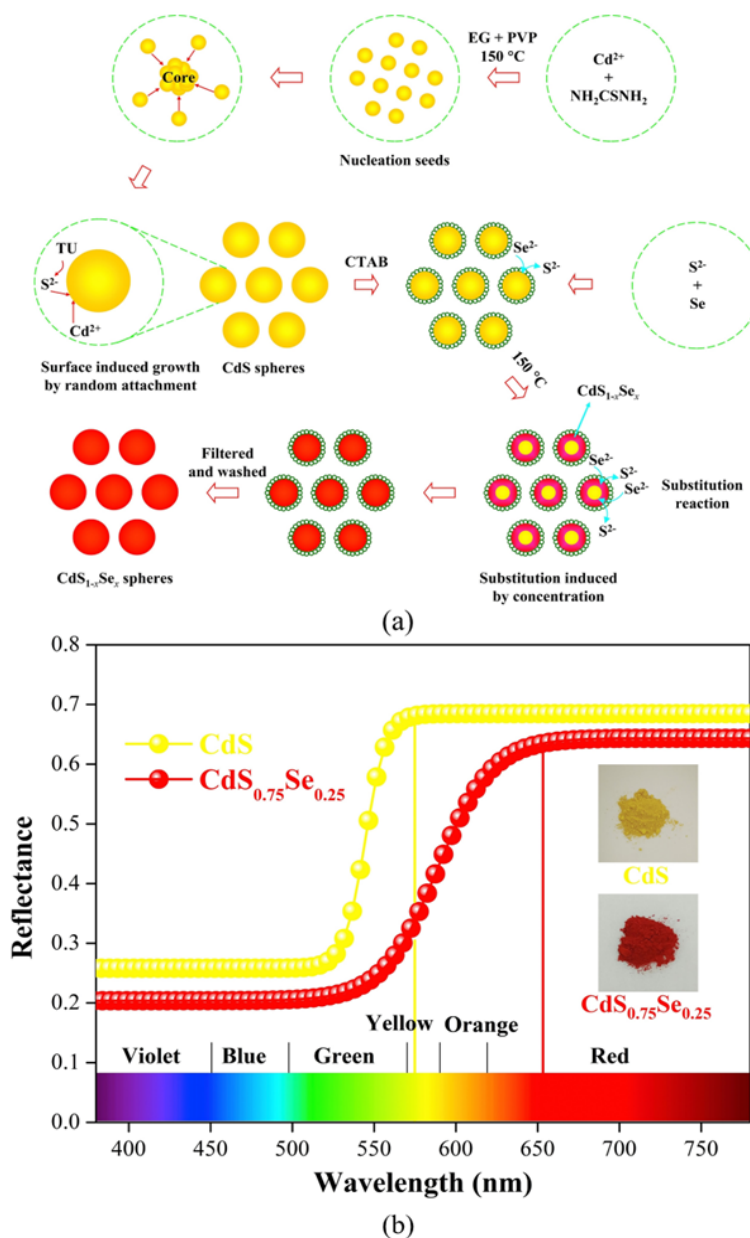
3.5. Cadmium sulphoselenide

Cadmium pigments represent the widest range of yellows and reds, among all inorganic pigments. The cadmium reds cover various shades of red, including light to deep oranges and bright to crimson and maroon reds [6]. Cadmium sulphoselenide ($CdS_{1-x}Se_x$, x=0–1) is an anion-doped solid solution, invented in 1919, which is claimed to be the only known intense bright red pigment, suitable for the ceramic industry [27, 28]. This pigment has a wurtzite structure with a hexagonal symmetry where cadmium ions are surrounded by the S^{2-}/Se^{2-} tetrahedrons (Fig. 4) [29]. The color tonality is adjusted by the amount of selenium dopant from yellow (x=0) to dark maroon (over 50% CdSe). Selenium decreases the band gap and the violet-blue reflection, leading to a more intense red color. Cadmium sulphoselenide pigments are insoluble in alkalis, water, and organic solvents, but they have a low acid resistance and thermal stability (below 600 °C). The details of the history of the cadmium sulphoselenide developments are reviewed elsewhere [28]. Cadmium, as a heavy metal, is a carcinogenic cumulative toxin, capable of affecting the kidneys, the respiratory, and the skeletal systems [30]. As
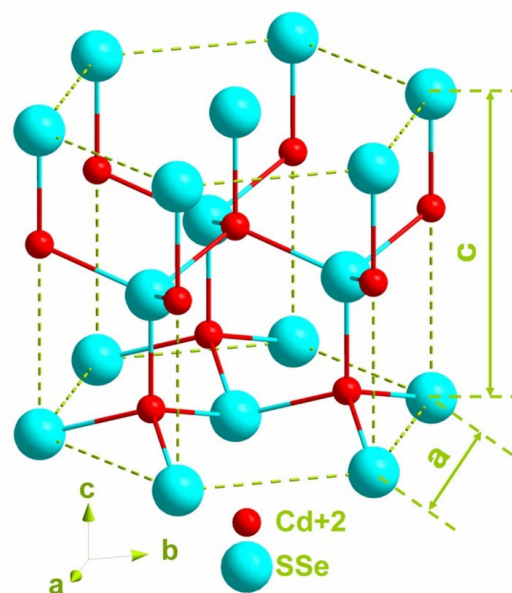
cadmium pigments have a low solubility in solvents, they were previously considered low-risk compounds for both the environment and humans, except in residential areas. However, a continuous photo-induced release of Cd^{2+} ions from the pigment in the microplastics and its leaching in water under simulated sunlight was reported by Liu et al. [31]. Also, it was stated that drinking glasses and toys are the most dangerous ones among cadmium pigment-containing products, due to the accessibility of cadmium ions in the glasses or the heavy metal exposure upon being chewed by children [30]. As cadmium sulphoselenide pigments are among the toxic compounds and the main scope of this review is devoted to environmentally friendly alternatives, only two recent research works [29, 32] are briefly reviewed in this section. However, the reader may reach out to the other research articles [33–37] for more information and details on the synthesis procedure and properties of cadmium sulphoselenide red pigments. Also, the safer encapsulated cadmium sulphoselenide pigments are brought in the red zircon pigments section.

Wu et al. [29] reported an in-situ formation of the spherical $CdS_{0.75}Se_{0.25}$ pigments in two steps. A scheme of the cadmium sulphoselenide formation is shown in Fig. 5a. At first, cadmium sulfide was synthesized using a solvothermal process. Then, the spherical CdS particles were added to the water-dissolved CTAB (template). The prepared Na_2S-Se solution was dropwisely added to the CTAB + CdS mixture. Then, selenium ions gradually replaced the sulfur anions in the cadmium sulfide and consequently, an in-situ formation of $CdS_{1-x}Se_x$ submicron particles occurred through an ion exchange and a surface-induced growth. The photos of the synthesized CdS and $CdS_{0.75}Se_{0.25}$ pigments along with the UV-Vis results are shown in Fig. 5b. The yellow cadmium sulfide pigments (L*=65.79, a*=2.49, and b*=50.81) exhibited a higher reflectance and a red-shift was seen in the case of $CdS_{0.75}Se_{0.25}$ (L*=47.76, a*=43.91, and b*=30.05) due to the band gap narrowing through doping. The lower reflectance of the cadmium sulphoselenide pigments was attributed to its larger particle

Fig. 5. a) A scheme of the in-situ formation of cadmium sulphoselenide pigments using the as-prepared CdS cores and b) UV-Vis reflectance plot of the obtained pigments. "Reproduced from Ref. [29] with permission from Elsevier. All rights reserved".

size. The uniform spherical morphology and the submicron size of the CdS and the CdS$_{0.75}$Se$_{0.25}$ particles are confirmed by the SEM images in Fig. 6a–d. So, the obtained pigments were suitable for the ink-jet applications.

Li et al. [32] synthesized ultra-red CdS$_{1-x}$Se$_x$ pigments using a hydrothermal process with different S/Se molar ratios (R = 0.67, 0.83, 1.00, 1.17, and 1.33). As the cadmium sulphoselenide is a semiconductor, the Tauc plots of the synthesized pigments were drawn in Fig. 7 for the band gap estimations and a better understanding of the obtained colors. The band gaps of the samples with R = 0.67, 0.83, 1.00, 1.17, and 1.33 were equaled to 2.00, 2.00, 1.95, 1.94, and 1.94 eV, respectively. The differences between the theoretical

(E_g = 2.28 and 2.12 eV for the Se dopant amounts of 0.25 and 0.429 mol) and the estimated values were attributed to the microscale crystals of the synthesized pigments versus the nanoscale sizes of the theoretical compound. Increasing the S/Se ratio resulted in narrower band gaps and consequently a red shift in the absorbance threshold. Therefore, the pigments with higher amounts of the selenium dopant showed a deeper red. The optimum sample was the one with R=1.00, as it showed the reddest color (L*=44.69 and a*=49.93). The average particle sizes of the obtained cadmium sulphoselenide pigments are shown in the SEM images of the samples in Fig. 8 the bigger the particle size the darker the red color was, another affective factor on the optical properties.
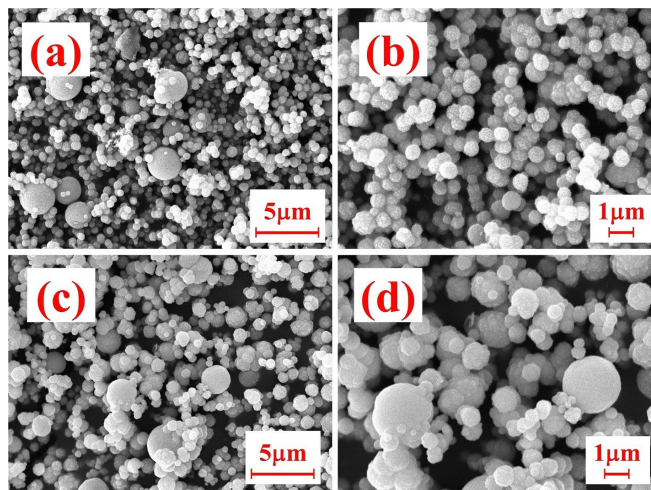
Fig. 6. SEM images of the synthesized a, b) cadmium sulfide and c, d) cadmium sulphoselenide pigments in low (*500) and high (*1000) magnifications. "Reproduced from Ref. [29] with permission from Elsevier. All rights reserved".

4. Environmentally friendly alternatives

4.1. Red perovskite pigments

Several perovskite compounds can be applied as pigments. Red perovskite pigments are considered high-temperature resistant environmentally friendly alternatives for toxic compounds with desirable optical properties. Currently, Cr-doped $YAlO_3$ is the only commercialized perovskite pigment [38] which was discovered in 1999 by Baldi and Dolen [39]. One year later, Jansen and Letschert [40] synthesized novel $Ca_{1-x}La_xTa(O, N)_3$ with red (x = 0.9–0.1) to (x = 0.3–0.75) orange colors, comparable to cadmium sulfoselenides [40].
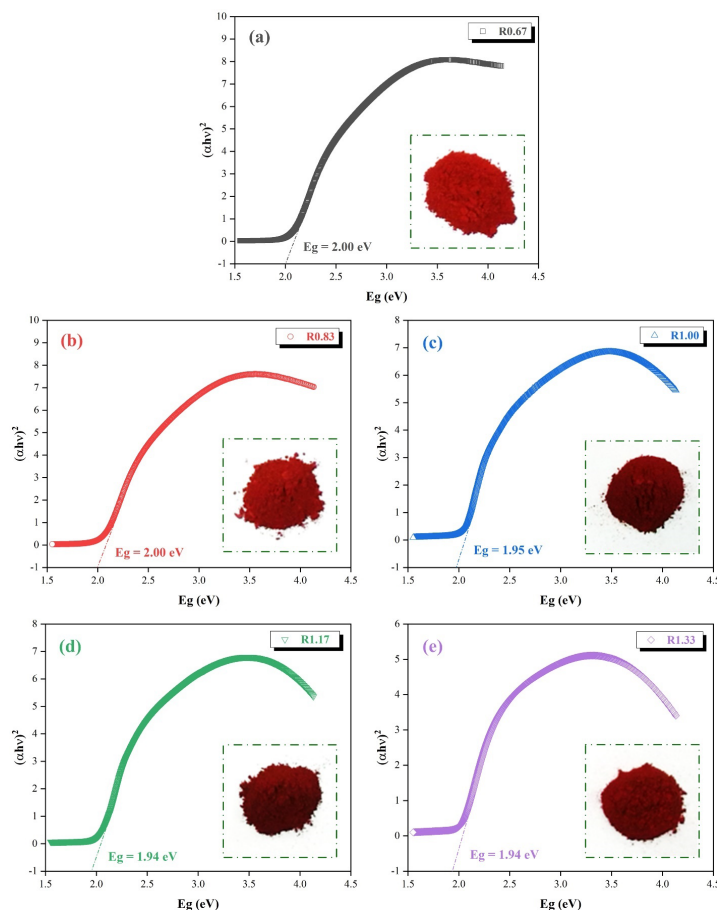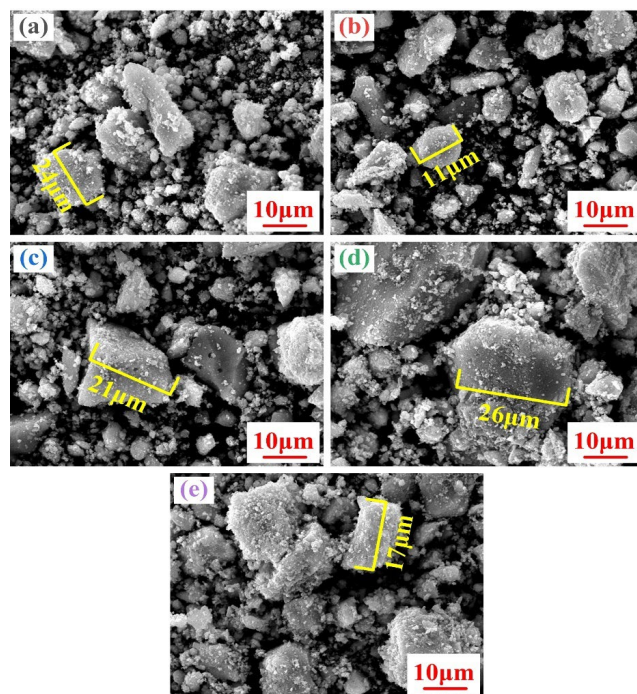

Fig. 7. The Tauc plots of the synthesized cadmium sulphoselenide pigments using a hydrothermal process with various S/Se ratios (indicated in the top-right of each image). "Reproduced from Ref. [32] with permission from Taylor & Francis Group. All rights reserved".

Fig. 8. SEM images of synthesized cadmium sulphoselenide pigments using a hydrothermal process with various S/Se ratios: a) 0.67, b) 0.83, c) 1.00, d) 1.71, and e) 1.33. "Reproduced from Ref. [32] with permission from Taylor & Francis Group. All rights reserved".

Chromium (IV) doped calcium titanate was also synthesized, but its characteristic color in a transparent glaze was red-brown [41]. Matteucci et al. [42] investigated the coloring mechanism of the perovskite red pigments using a wide range of samples ($AAl_{2-x}Cr_xO_3$; A=Nd, Eu, Dy, Y, Sm, Yb, Er, Ho, and Gd; x = 0.035) by the UV-Vis-NIR, the CIE-Lab, and the XRD techniques. Various symmetries and cell parameters were obtained after introducing different rare earth elements into the A-site of the perovskite structure (ABO_3) and the symmetry reduced with a shift from hexagonal (Nd-perovskite) to orthorhombic (Sm-Yb perovskites). The larger lanthanide ionic radiuses increased and decreased the A-site and B-site volumes (the chromium place), respectively. An octahedral tilting distortion was a result of the B-site contraction, lowering the Al-O interatomic distance. There was an inverse relationship between the interatomic distance and the crystal field strength ($\Delta = k (Al - O)^{-5}$). So when the (Al, Cr)-O distance reduced, the red color became more intense.
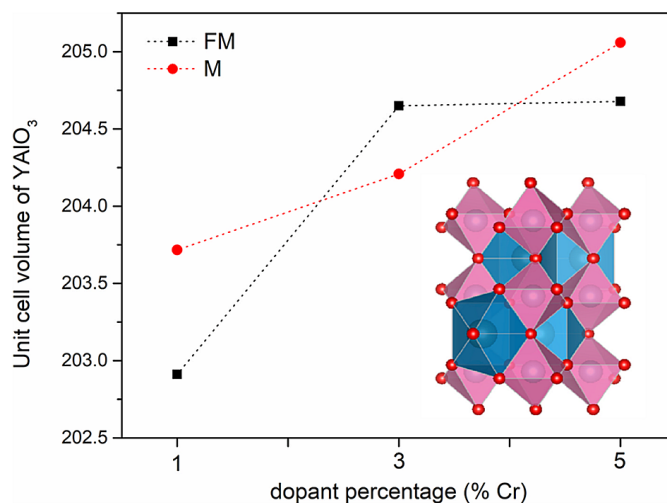

Fig. 9. The $YAlO_3$ unit cell volume in the FM (free of mineralizer) and M (mineralizer-containing) systems. "Reproduced from Ref. [45] with permission from Elsevier. All rights reserved".
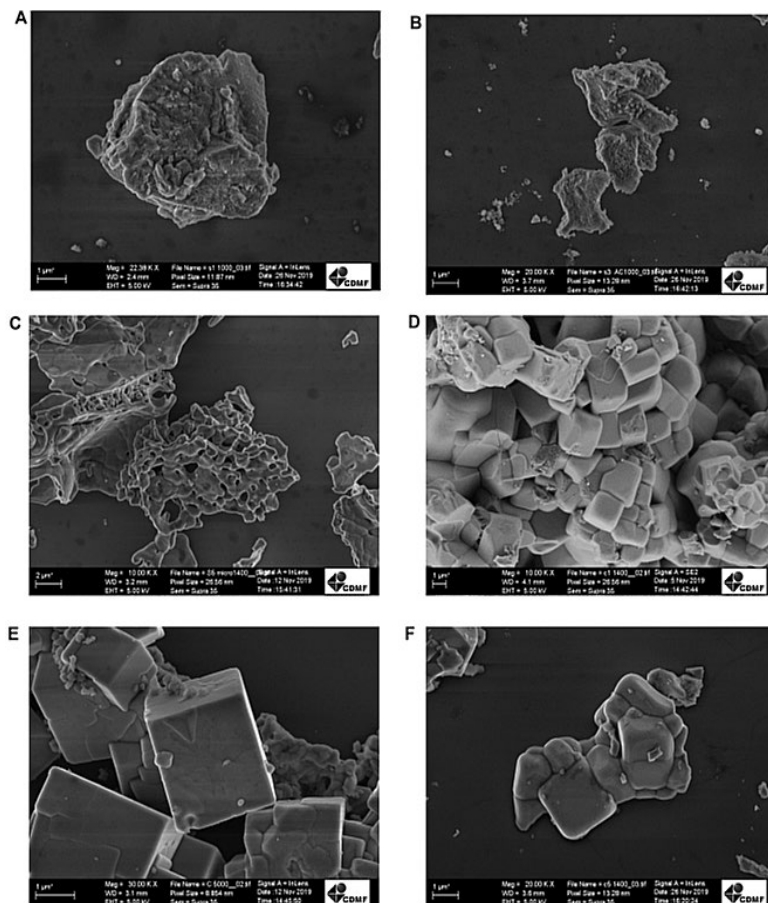
Fig. 10. FEG-SEM micrographs of the samples (FM: free of mineralizer, M: mineralizer-containing): a) FM-1%, b) FM-3%, c) FM-5%, d) M-1%, e) M-3%, and f) M-5% after being heat-treated at 1400 °C. "Reproduced from Ref. [45] with permission from Elsevier. All rights reserved".

Due to the requirements of prolonged heat treatments with high temperatures over 1800 °C for perovskite formation, mineralizers are essential and inevitable part of the synthesis process [43]. Ahmadi et al. [44] evaluated the effect of mineralizer type, the amount of chromium dopant, the fuel-to-oxidizer ratio, and the soaking time on the chromium-doped
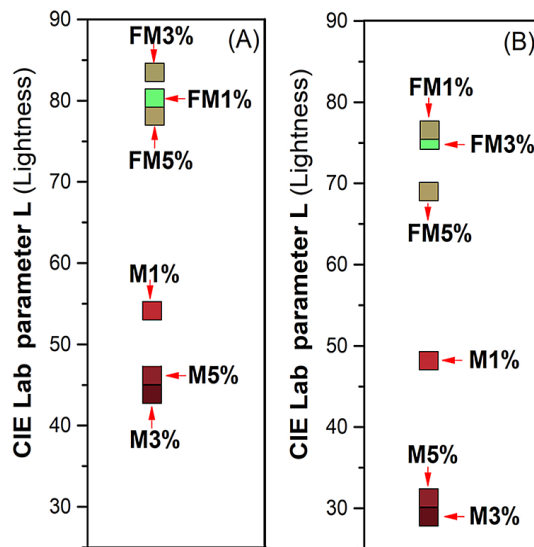
Fig. 11. Effects of the dopant and mineralizers on a) the redness (a*) and b) luminosity (L*) of the ceramic pieces after being glazed using the synthesized pigments. "Reproduced from Ref. [45] with permission from Elsevier. All rights reserved".

$YAlO_3$ pigments, and the optimum results were obtained with 0.03 mol Cr using a $NaF:MgF_2:Li_2CO_3$ (3:2:1) mineralizer system at a calcination temperature of 1400 °C for 4 h in the fuel-rich sample. Marques et al. [45] synthesized Cr^{3+}-doped (0.01, 0.05, and 0.07 mol%) yttrium aluminate perovskite pigments via a chemical combustion method with and without using $MgF_2-Na_2B_4O_7$ as a mineralizer and compared the results. The unit cell structure and volume are represented in Fig. 9. Y cations formed a cell that was surrounded by 10 oxygen anions, resulting in dodecahedral $[YO_{10}]$ clusters. Also, 6 oxygen anions coordinated the aluminum cations and the octahedral $[AlO_6]$ clusters were formed. A moderate expansion was seen in both mineralizer-containing (M samples) and free-of-mineralizer (FM samples) systems, attributed to the chromium entrance to the lattice. FEG-SEM images of all samples are shown in Fig. 10a–f. The mineralizer-free samples (Fig. 10a–c) were irregularly shaped and porous. The pores were related to gas exhaustion during the combustion process. However, the other pigments (Fig. 10d–f) were mostly agglomerated cubic particles due to the mineralizer modifications and their effects on the crystallization temperature. Increasing the dopant amount led to reduced particle sizes which was more pronounced in the mineralizer-free pigments. The redness values (a*) were higher in the mineralizer-containing samples due to the electronic cloud distortion by fluorine. However, the luminosity (L*) decreased, revealing the darker color of the mineralizer-containing pigments. But it enhanced after glazing. The related CIELab results are depicted in Fig. 11.

In addition to the above-mentioned factors, synthesis methods can also affect the chromaticity of the perovskite red pigments. In a comparative study, Miguel et al. [46] synthesized $Y_{0.98}Al_{0.98}Cr_{0.04}O_3$ perovskite pigments using the solid-state and the coprecipitation methods and calcined them with conventional and microwave-assisted heat treatments. The colorimetric results of the traditional route-derived pigments indicated lower L* (60.50) and higher a* (36.06) values than the coprecipitation-derived ones (L*=60.98, a*=28.33). Because the coprecipitation method contributed to the formation of unwanted phases (garnet) and the obtained products were no longer pure perovskites. SEM images of the obtained pigments are shown in Fig. 12. The pigments obtained by the solid-state route showed a cubic morphology with aggregated crystals in a size range of 1–2 μm. However, the coprecipitation-derived ones were highly sintered and partially melted with a crystal size below 1 μm and lost their color after glazing.

Red perovskite pigments can also be applied in cool applications. In a recent study, instead of doping chromium, Blasco-Zarzoso et al. [47] developed sustainable $YAl_{1-x}Fe_xO_3$ pigments (x=0, 0.25, 0.5, 0.6, 0.75, and 1) with a wide color range from yellow to red as well as NIR reflecting properties for cool applications. The red color was obtained in the $YFeO_3$ composition (L*=36.86, a*=22.39, b*=16.66, and c*=27.54). These pigments showed good stability in a commercial glaze and could reduce the building temperature by 4–5 °C. Bae et al. [1] synthesized environmentally friendly non-toxic orange Sr_4Mn_2 $(Cu_{1-x}Zn_x)O_9$ (x=0, 0.5, and 1) hexagonal perovskite pigments with a high NIR reflectivity. In another study [48], $Ba_2RE_{1-x}Ce_xTaO_6$ (RE=La, Gd, Y; x=0, 0.1, 0.2, 0.3, 0.5, and 1) double-perovskite pigments were synthesized using a solid-state method. The highest redness was achieved in the $Ba_2La_{0.3}Y_{0.2}Ce_{0.5}TaO_6$ pigments (L*=49.3, a*=39.0, and b*=35.9), lower than the cadmium red (a*=60.4) but higher than the Bengal red (Fe_2O_3) (a*=32.2). The chromaticity properties of some perovskite pigments seen in the literature are represented in Table 2 and compared to cadmium red. None can compete with the redness value of cadmium red, but the researchers, aiming to improve and develop environmentally friendly red perovskite pigments with vivid color, have reached a milestone.

Table 2. Examples of the red perovskite pigments in the literature compared to the cadmium red.

No.	Chemical composition	Dopant (mol)	Chromaticity properties			Color	References
			L*	a*	b*		
1	$YFeO_3$	-	36.86	22.39	27.54	Red	[1]
2	$YAlO_3$	Nd, Cr (0.05, 0.05)	39.60	25.39	16.88	Red	[27]
3	Cadmium Red (CdS.Se)	-	41.10	65.21	56.84	Red	[40]
4	$CaTaO_2N$	La (0.6)	47.60	37.26	67.00	Orange-red	[40]
5	$LaTaON_2$	-	26.35	37.01	30.08	Red	[40]
6	$YAlO_3$	Fe (0.75)	63.78	14.96	37.03	Brownish-red	[47]
7	$YAlO_3$	Cr (0.03)	47.69	31.05	18.96	Red	[49]
8	$YAlO_3$	Cr, Mg (3, 2)	54.55	34.05	26.16	Coral-red	[50]
9	$YAlO_3$	Cr, Ca (3, 0.5)	55.64	35.41	25.92	Red	[51]
10	$TbFeO_3$	-	33.84	20.97	16.65	Reddish-orange	[52]
11	$GdFeO_3$	-	54.99	19.14	23.64	Red	[53]
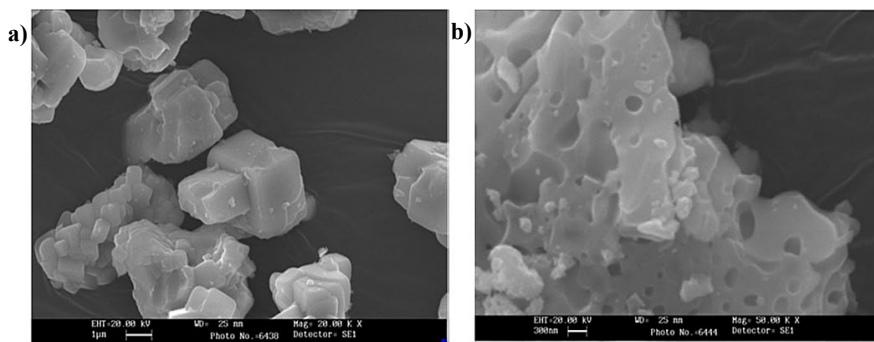
Fig. 12. SEM images of the chromium-doped $YAlO_3$ red pigments synthesized at 1400 °C using a) the ceramic route and b) the coprecipitation route. "Reproduced with permission from Ref. [46]".

4.2. Iron oxide/hydroxide red pigments

Iron oxides and hydroxide pigments applications have been used from prehistoric (seen in cave paintings) and ancient eras up to now. Iron oxide pigments, whether natural or synthetic, are of great importance in the pigment industry, due to low production costs, a wide range of colors (yellow, orange, red, brown, and black), chemical stability, and above all nontoxicity[2]. Čiuladienė et al. [54] investigated three classic iron-based red pigments including hematite (Fe_2O_3), red ochre (Fe_2O_3), and red bolus ($Fe_2O_3.xSiO_2.yAl_2O_3$) in various binding media. The digital images of these iron pigments and the applied binding media before and after aging are shown in Fig. 13. The red ochre showed a deep red color, while hematite was red-brown. The red bolus was the most stable one and showed the lowest color changes after aging. The particle size of almost every sample decreased after aging.

Mufti et al. [55] synthesized red (hematite), yellow (goethite), and black (magnetite) pigments using iron sand. The coprecipitation method (with pH alterations) was applied for the black and yellow pigments, while the red one was obtained by a solid-state method at 400 °C and 700 °C for 1h. Increasing the temperature for the hematite calcination and enhancing the pH value for the goethite led to particle growth in each. But all synthesized iron pigments were nano-scaled.

Hashimoto et al. [56] obtained α-Fe_2O_3 red pigments using a hydrothermal treatment with lead-free overglaze enamel applications. As the lead-free frits give a duller red color compared to the leaded ones, more intense red pigments are required. The optimum pigment was a hematite sample, heat-treated at 90 °C with the brightest red and the best performance in the lead-free glazes.

4.2.1. Ferrite pigments

Iron-based mixed metal oxides are nontoxic magnetic materials with significant physical and chemical properties [8]. Bismuth ferrite ($BiFeO_3$) is a multiferroic substance with a perovskite structure and wide applications in photocatalysts, optoelectronic devices, detectors, etc. But bismuth is easily evaporated during the production process and leaves some vacancies behind, destabilizing the structure together with iron valence fluctuations. James et al. [5] synthesized $Bi_{1-x}M_xFeO_3$ (M = Y, La) pigments with a reddish-brown color using a simple solid-state route. Y^{3+} and La^{3+} additions stabilized the rhombohedral perovskite $BiFeO_3$ structure and slightly changed the band gap from 1.95 eV to 2.23 eV. Doping yttrium and lanthanum into the structure of bismuth ferrite changed the cold brown color to vivid red-browns.

Calcium ferrite ($CaFe_2O_4$) is a red-brick coloring material with a spinel structure with high thermal and chemical stabilities (especially, against
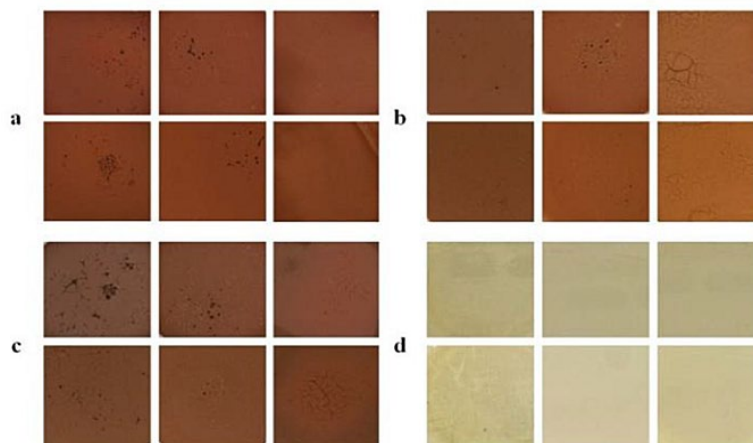
Fig. 13. Digital photos of a) red ochre, b) red bolus, c) hematite, and d) (left to right) gum Arabic, fish glue, and parchment glue before (top) and after (bottom) aging for 35 days. "Reproduced with permission from Ref. [54]".

(a)   (b)
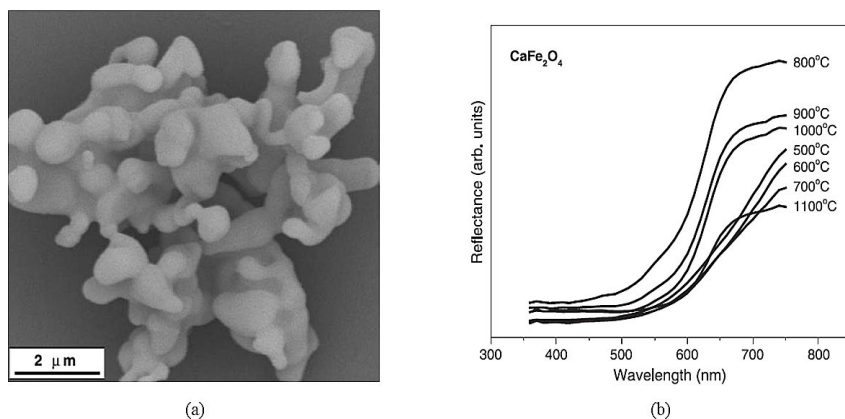
Fig. 14. a) SEM image of CaFe$_2$O$_4$ pigment synthesized at 1000 °C using a polymer precursor route and b) DRS results of CaFe$_2$O$_4$ pigments at various temperatures. "Adopted from Ref. [57] with permission from Elsevier. All rights reserved".

glaze materials). Canderia et al. [57] synthesized calcium ferrite red spinel pigments using a polymeric precursor (Pechini) route and investigated their stability under industrial conditions. In this process, a metallic citrate is polymerized using ethylene glycol. The chelating agent is a hydrocarboxylic acid in an aqueous solution. Esterification occurs using a polyalcohol. Finally, a homogenous resin containing metal ions is obtained through heating. Increasing the temperature resulted in higher particle sizes. This was attributed to the presence of nanoparticles, contributing to the agglomeration (Fig. 14a). According to the DRS spectra in Fig. 14b, a characteristic band (650 nm) is seen at calcination temperatures above 800 °C in the fully crystallized monophase spinel samples, indicating the dark red color (L*=47.450, a*=20.645, b*=56.894 at 800 °C). The pigment color was dependent on the oxidation state of the chromophore and was stabilized at 800–1000 °C.
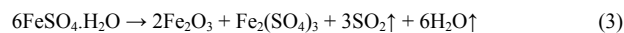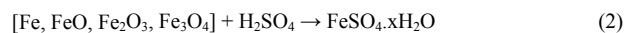
4.2.2. Composite iron oxide pigments

Hashimoto et al. [7] synthesized hematite/alumina composite pigments with a porous disk-like structure and a yellowish-red color using a wet chemical process at 700 °C. A bright yellowish color (L*=48.3, a*=37.2, and b*=48.8) was seen in the pigment-containing 0.3 mol Al, attributed to the unique porous structure. The colorimetric results were 1.25, 1.22, and 2.32 times higher than the commercial hematite, respectively. This pigment showed a high thermal stability up to 1100 °C. Lu et al. [58] synthesized environmentally friendly clay (illite/smectite, rectorite, kaolinite, montmorillonite, vermiculite, sepiolite, halloysite, and illite-rich clay) -iron oxide hybrid pigments via a hydrothermal method. The surface silanol groups, charges, and solid acid sites of the clays are the decisive factors for the obtained colors. The clay minerals, as the microreactors, induced the in-situ formation of iron oxide crystals and restricted the particle aggregation. The best pure red color was obtained in the illite-containing pigments (L*=31.8, a*=35.2, b*=27.1, and c*=44.4) with high chemical and thermal stabilities.

4.2.3. Waste-derived iron oxide pigments

Mill-scale is the iron oxide layer formed on the steel slabs during the heating process, easily removed by showering. Researchers aim to find applications for the iron-rich, low-impurity, and chemically stable mill-scale that is usually dumped in landfills without recycling. Saiful

Quddus et al. [59] synthesized pigment-grade maroon red iron oxide flakes with an acceptable purity (95.3%) from the mill-scale using a multi-step process: (1) milling, (2) acid treatment, (3) application of redox agents, and (4) calcination. Almost every step was repeated multiple times. The application of sodium hydrosulfite dihydrate as the redox agent and selection of the iron-to-sulfuric acid molar ratio of 1:2.39 resulted in an optimum bright glossy pigment. The redox reactions that occurred during the hematite pigment production from mill-scale are as follows:

$$[Fe, FeO, Fe_2O_3, Fe_3O_4] + H_2SO_4 \rightarrow FeSO_4.xH_2O \tag{2}$$

$$6FeSO_4.H_2O \rightarrow 2Fe_2O_3 + Fe_2(SO_4)_3 + 3SO_2\uparrow + 6H_2O\uparrow \tag{3}$$

$$Fe_2(SO_4)_3 \rightarrow Fe_2O_3 + 3SO_3\uparrow \tag{4}$$

Fiuza et al. [60] developed iron-based pigments from the purified scum ashes. The scum was heat-treated to produce the required ashes. The obtained pigments showed an orange color at 950 °C and a dark red at higher temperatures. In addition to the non-toxic composition of the obtained pigment, the synthesis process is also environmentally friendly as it helps to recycle the sewage, reducing environmental pollution.

4.3. Cerium oxide pigments

Cerium oxide powder is a nontoxic inorganic pigment with high thermal and chemical stabilities [61]. It has a pale yellow color but is tunable with doping other metallic elements such as praseodymium in its cubic fluorite-like lattice. Ceria has a strong absorption below 400 nm, due to the O$_{2p}$-Ce$_{4f}$ transitions, contributing to its yellow color which becomes white during the heating process (a decreased b*). This material is a good matrix for praseodymium ions (Pr^{3+} or Pr^{4+}). Depending on the dopant amount, synthesis, and annealing conditions, various colors such as red-brown, orange, or magenta are seen for this composition [62].

Nurhasanah et al. [61] synthesized pure and iron-doped ceria nanopowders using a precipitation method. The cubic fluorite structure of cerium oxide was confirmed in the obtained spherical particles. As usual, the cerium oxide powder was pale yellow, but it changed to a brick-red color after doping. According to the UV-Vis results, the bandgap became wider after iron doping. Iron also affected the crystallite size and the surface area of the pigment, reducing the former
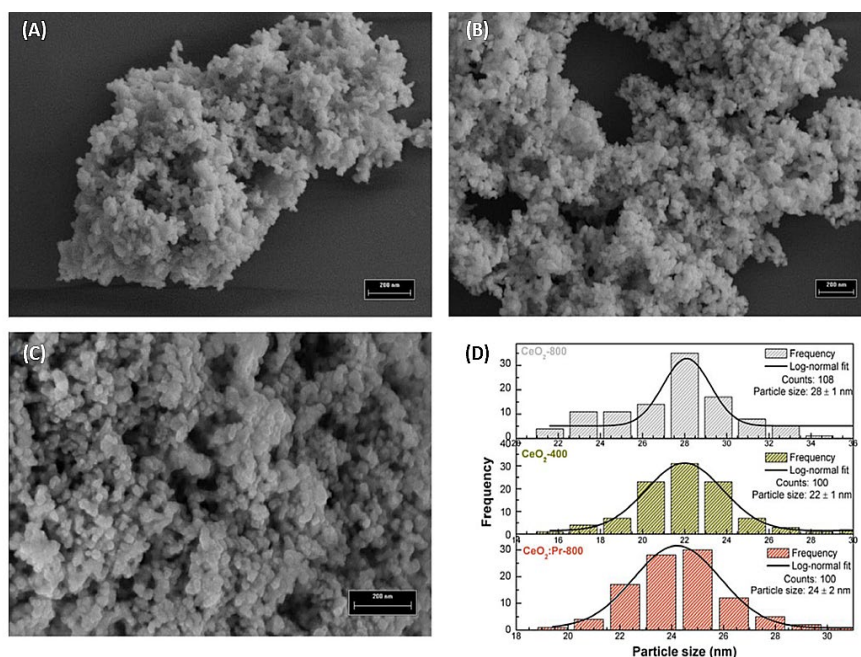
Fig. 15. FESEM micrographs of pure and doped ceria pigments synthesized at various temperatures: a) CeO$_2$ (400 °C), b) CeO$_2$ (800 °C), c) CeO$_2$:Pr (800 °C) and d) particle size distribution. "Reproduced from Ref. [62] © 2020 The American Ceramic Society, with permission from John Wiley and Sons".

and increasing the latter. Mićović et al. [4] synthesized non-toxic dark red (praseodymium doped) and pink (erbium-doped) cerium oxide-based ceramic nano pigments using a self-propagating room temperature method and a follow-up heat treatment at 600, 900, and 1200 °C for 15 min and recommended them as alternatives for the currently used toxic pink and red pigments in the coatings, cosmetics, glass enamels, plastics, and ceramic industries. The particle size and pigment color depended on the temperature of the heat treatment. However, the obtained pigments maintained their thermal stability up to 1200 °C. Gonzaga et al. [62] synthesized yellow (pure) and red

(praseodymium) nanocrystalline cerium oxide pigments using a polymeric precursor method. SEM images shown in Fig. 15 confirmed the nanoscale particle sizes (22–28 nm) and their dependency on the annealing temperature. However, doping did not significantly affect the particle size of the pigments. A uniform particle size distribution was detected in all samples (Fig. 15d). UV-Vis reflectance spectra of the obtained pigments at various temperatures are shown in Fig. 16. The pure cerium oxide showed a pale-yellow color (due to a blue absorption) which turned into white upon annealing. This was attributed to the promotion of oxygen vacancies during the heating
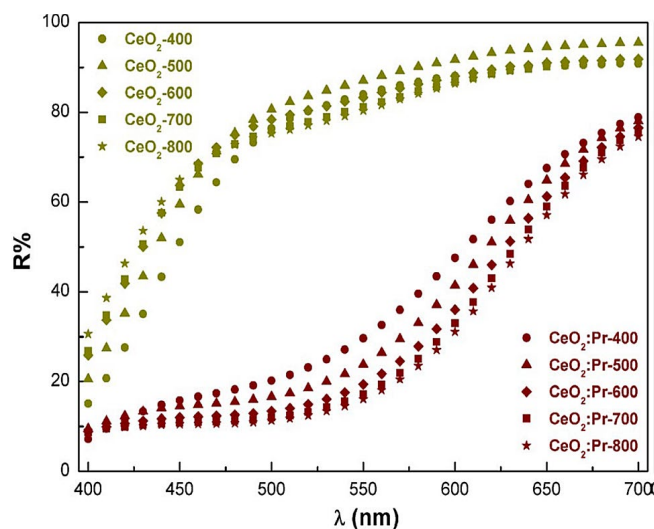
Fig. 16. DRS results of CeO$_2$ and CeO$_2$:Pr pigments as a function of the annealing temperature. "Reproduced from Ref. [62] © 2020 The American Ceramic Society, with permission from John Wiley and Sons".

process. Pr-doped cerium oxide pigments showed a red-orange color, attributed to $4f^2 \rightarrow 5d^1$ transitions of Pr^{3+}. Praseodymium doping reduced the bandgap by introducing a new energy level in it. Increasing the temperature, a shift toward higher wavelengths was seen. The result was a red-orange to red-brown color change. This was also attributed to the formation of oxygen vacancies during annealing and the preferred localization of the left electrons on Pr atoms. Kumari et al. [63] synthesized environmentally friendly $Ce_{0.95}Pr_{0.05-x}M_xO_2$ (M = Mn, Si) red pigments using a solid-state route. The Si^{4+} dopant shifted the absorption spectra toward the blue region and gave a bright red-brown color, while the Mn^{4+} doping resulted in the absorption edge stabilization and a dark brown color. Radhika et al. [64] synthesized $Ce_2Pr_{0.2}Fe_xO_{4.3+y}$ red-brown pigments with an average particle size of 150 nm using an ethylene glycol-based sol-gel method at 800 °C for 2 h. The obtained pigments had a high near-infrared reflectance (82.7%), potentially ideal for cool coating applications. Aruna et al. [65] synthesized $Ce_{1-x}Pr_xO_{2-\delta}$ (x = 0–0.5) red ceramic pigments with a reflectance edge at about 690 nm by a combustion method. The application of ammonium acetate as the fuel led to a controlled combustion reaction and a particle size of 7–12 nm without any mineralizer requirements.

In a novel study, Llusar et al. [66] synthesized terbium-doped ceria red ceramic pigments instead of using the regular praseodymium and investigated the effect of different synthesis methods (including a conventional solid-state method, a classical coprecipitation, and homogenous precipitations using microwave or ultrasonic irradiations) on the chromaticity. An optimum composition ($Ce_{0.9}Tb_{0.1}O_{0.2}$) with a nice red color at 1500 °C was determined and selected for these investigations, synthesized using the solid-state method. The classic coprecipitation also gave a very intense red color at 1500 °C, but poor quality was obtained below that temperature. Optimization of the synthesis method resulted in better red colors at lower temperatures with a similar coloring performance (L* = 53–59, a* = 22–25, and b* = 29–34) to the praseodymium doped ceria in the glazes.

4.4. Cerium trisulfide pigments

Although $CdSe_{1-x}S_x$ is a popular bright red pigment, its applications are restricted due to the presence of cadmium in the structure. Ce_2S_3, as a sesquisulfide compound, is gradually replacing $CdSe_{1-x}S_x$ pigments. There are many reasons for this substitution, including the abundance of cerium in the earth's crust, intense tinting properties, and lack of toxic elements in the composition [67]. Sesquisulfide compositions are often characterized by more than one phase. For example, cerium trisulfide (Ce_2S_3) has three phases, namely α, β, and γ. Each of these phases has distinct colors and structures and occurs at different temperatures. Black-brown or orange color with an orthorhombic structure is related to α-Ce_2S_3, obtained at below 900 °C. Meanwhile, β-Ce_2S_3 occurs at above 900 °C with a tetragonal structure and a burgundy color, and the cubic γ-Ce_2S_3 is formed with a dark red color at above 1200 °C. The γ-phase is of significant interest in the world of red pigments, due to its optical stability, excellent coloring performance, weather resistance, safe nature, and being environmentally friendly [68].

Contrary to the mentioned advantages, γ-Ce_2S_3 pigment has low thermal stability at temperatures above 350 °C which eases its oxidation and discoloration and restricts its applications in the ceramic industry [69]. This thermal instability rises from the γ-Ce_2S_3 defective

crystal structure. A cubic Th_3P_4-type structure full of vacancies along with highly oxophilic cerium ions craves oxygen ions, leading to low thermal stability [70]. Many strategies have been applied to improve the thermal instability and discoloration of γ-Ce_2S_3 at high temperatures. Among them, doping has been applied in many studies to improve the thermal stability of γ-Ce_2S_3 pigments [67, 71–75], as the dopants occupy the vacancies improve the structural stability, and also facilitate a low-temperature synthesis. On the other hand, adjusting the preparation process using new precursors or novel synthesis routes is another way to improve the thermal and optical properties of γ-Ce_2S_3 pigments.

4.4.1. Doped γ-Ce_2O_3 pigments

Li et al. [72] investigated the effect of Ba^{2+} doping ($n_{Ba/Ce}$=0, 0.1, 0.2, 0.3, 0.4, 0.5, and 0.6) on thermal stability and physical and optical properties of γ-Ce_2S_3 pigments. When $n_{Ba/Ce}$=0-0.5, a pure γ-Ce_2S_3 phase was obtained via a calcination process at 900 °C for 150 min, but a new heterogeneous phase (BaS) was obtained using higher amounts of Ba^{2+}. Increasing the $n_{Ba/Ce}$ molar ratio enhanced the band gap from 2.06 to 2.31 and shifted the color from red to orange-red and at last to yellow. Maximum redness was seen in the sample with a Ba/Ce ratio of 0.1 (L*=33.51, a*=37.07, b*=27.18) and it maintained its chromaticity at 440 °C. In a similar study, Li et al. [67] synthesized the Ba^{2+}-Sm^{3+} co-doped γ-Ce_2S_3 red pigments using the coprecipitation method at 850 °C for 150 min. CS_2 was used as a sulfur source, while the ratio of $n(Ba)/n(Ce_{1-x}Sm_x)$ = 0.1 was maintained. X amounts were 0, 0.01, 0.03, 0.05, and 0.1 mol. The result was a pure γ phase whose color shifted from red to red-orange with an enhanced Sm^{3+} amount (Fig. 17a). Because the band gap of the pigment changed from 2.12 to 2.14 eV. The band gap is a determining factor for the pigment color, as it shows the maximum energy caused by the electron-hole recombination and consequently the shortest color wavelength. The sample doped with 0.01 mol samarium had the best chromaticity. The optimum pigment was examined in terms of thermal stability using the TGA technique. The regular γ-Ce_2S_3 pigment is usually stable up to 350 °C, then it starts to dissociate into CeO_2 and SO_2. However, the 0.01 Sm-doped pigments did not experience any significant weight loss up to 440 °C. The reason for this improved thermal stability was attributed to the stabilizing role of the Barium dopant by filling the vacancies and forming a solid solution. Also, for further validations of thermal stability, the Ba^{2+}, Sm^{3+} co-doped sample was calcined at 400, 420, and 450 °C. Only above 440 °C, the oxygen absorption occurred and a heterogenous phase ($Ce_2O_2S_2$) was formed. Before that, a high redness (L*=21.79, a*=22.19, b*=27.15, and c*=35.06) was maintained up to 440 °C and only a pure γ phase was present (Fig. 17b).

Gao et al. [70] synthesized Pr-doped γ-Ce_2S_3 (dopant amounts of 0.01, 0.05, 0.1, and 0.15) red pigments from a Pr-containing CeO_2 precursor using a combined hydrothermal-sulfurizing method. Praseodymium changed the color of γ-Ce_2S_3 pigments but it also enhanced thermal stability significantly. When 0.10 mol praseodymium was doped in the structure, the pigment could tolerate high temperatures up to 470 °C and maintained its red color, but the pure γ-Ce_2S_3 became grey at 380 °C. There are two reasons for this phenomenon: a better thermal resistance provided by praseodymium sulfide and a lattice distortion caused by the introduction of Pr^{3+} that prevents dislocation movements. Chromaticity values of Pr-doped γ-Ce_2S_3 pigments with various amounts of dopant at different calcination temperatures are represented in Table 3 [70].
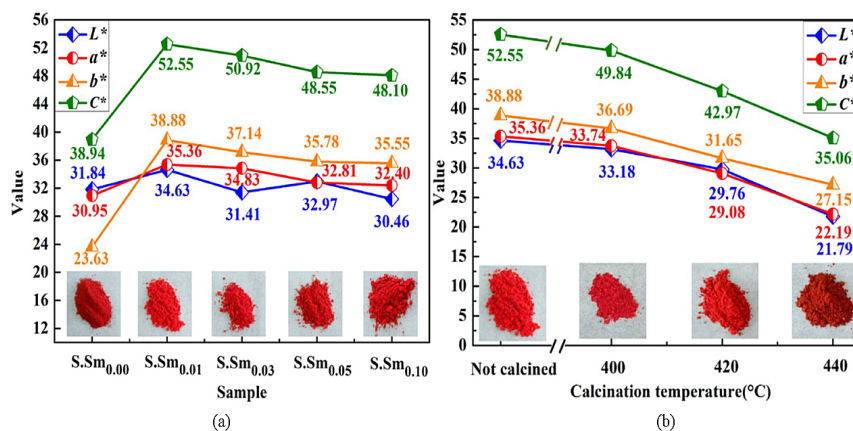
Fig. 17. Colorimetric results of a) Ba^{2+}, Sm^{3+} co-doped γ-Ce_2S_3 red pigments with various amounts of Sm^{3+} and b) the optimum sample containing 0.01 mol Sm^{3+} dopant calcined at various temperatures. "Adopted from Ref. [67] with permission from Elsevier. All rights reserved".

Song et al. [74] synthesized lithium-doped γ-Ce_2S_3 red pigments with various Li/Ce ratios (n=0.05, 0.10, 0.15, 0.20, 0.25, and 0.30) via a simple gas-solid method. Lithium carbonate, cerium oxide, and carbon disulfide were mixed, ground, and placed in a tubular furnace in a CS_2/Ar stream at 900 °C for 4 h with a heating rate of 5 °C/min (Fig. 18). Lithium entered the γ-Ce_2S_3 lattice and formed a solid solution successfully. Increasing the $n_{Li/Ce}$ up to 0.20 decreased the lattice parameters and the two nearest Ce-S bond lengths, through the substitution of lithium ions for cerium. These amounts were maintained above $n_{Li/Ce}$=0.20, indicating the full-filled lattice vacancies and the band gap increased from 1.95 eV to 2 eV and a slightly shifted red color. Cerium polysulfide impurity was detected in the Raman spectroscopy results as the reason for the observed dark color in the obtained pigments. The γ-[Li]-Ce_2S_3 pigments with $n_{Li/Ce}$=0.20 could tolerate high temperatures up to 450 °C and maintain their red color (Table 4). In a similar study, Li et al. [71] studied the effect of potassium doping on the structure and properties of γ-Ce_2S_3 pigments. When the K/Ce ratio was above 0.25, a heterogenous phase ($KCeS_2$) was formed. The lattice parameters increased when K/Ce was in a range of 0–0.25, but they remained unchanged after that, meaning all

vacancies were filled with dopants. When the level of K doping increased, the color shifted from red to orange and finally yellow (Fig. 19). When K/Ce=0.10, the redness value (a^*) was maximized (L*=33.86, a*=36.68, and b*=38.15) and it was maintained at high temperatures up to 420 °C.

In another study, Li et al. [75] synthesized Sr^{2+}, Dy^{3+} co-doped γ-Ce_2S_3 using a combined coprecipitation-sulfurization method and investigated thermal stability and colorimetric parameters. XRD results confirmed the entrance of Dy^{3+} ions into the lattice and a solid solution formation. The band gap remained the same after doping (2.01–2.04 eV). The optimum sample with a Dy^{3+}/Ce^{3+} ratio of 0.15 and the best red color (L*=31.49, a*=30.94, b*=25.33) could preserve its chromaticity at 410 °C. The UV-Vis results showed an absorption band around 530 nm attributed to the electron transitions of Ce 4f→Ce 5D in the γ-Ce_2S_3 and a 70% reflectivity around 700 nm, indicating a bright-red color (Fig. 20). The authors stated that reasons for selection of this dopant combo were the abilities of Sr^{2+} in reducing the synthesis temperature and Dy^{3+} in providing thermal stability.

Table 3. Chromaticity values of Pr-doped γ-Ce_2S_3 pigments with various amounts of dopant at different calcination temperatures. "Redrawn from Ref. [70] with permission from Springer Nature. All rights reserved".

No.	L*	a*	b*	photo
S,S0	30.48	32.25	18.93	
S,S0.01	26.20	27.57	14.66	
S,S0.05	26.53	28.38	13.23	
S,S0.10	29.16	30.13	16.81	
S,S0.15	26.84	29.42	15.77	
S,S0-380air	38.09	6.78	11.51	
S,S0.1-380air	29.14	30.13	16.81	
S,S0.1-460air	29.14	30.13	16.81	
S,S0.1-470air	25.58	29.47	17.27	
S,S0.1-480air	29.35	22.51	5.44	

Table 4. Chromaticity values of γ-[Li]-Ce_2S_3 pigments at various temperatures. "Redrawn from Ref. [74] with permission from Elsevier. All rights reserved".

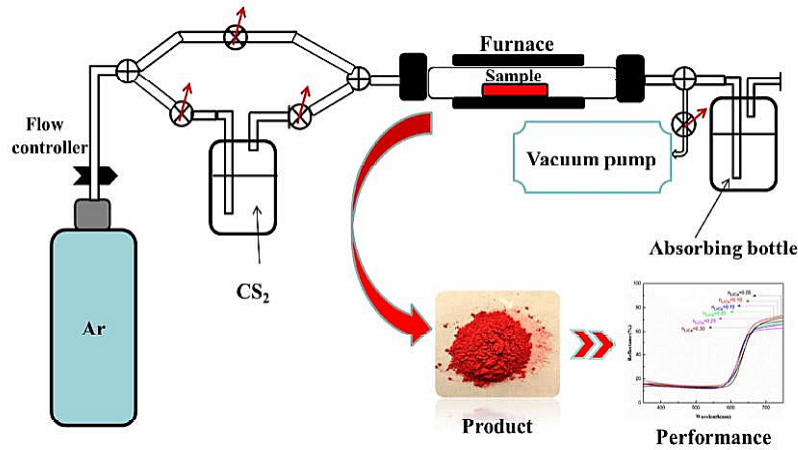| Sample	L*	a*	b*	Photo
350 °C ($n_{Li/Ce}$=0.05)	25.58	29.23	13.27	
400 °C ($n_{Li/Ce}$=0.05)	25.16	28.89	14.25	
450 °C ($n_{Li/Ce}$=0.05)	20.57	17.89	12.53	
350 °C ($n_{Li/Ce}$=0.20)	27.23	32.56	14.01	
400 °C ($n_{Li/Ce}$=0.20)	28.16	31.55	14.03	
450 °C ($n_{Li/Ce}$=0.20)	25.67	30.45	12.36	
460 °C ($n_{Li/Ce}$=0.20)	24.25	16.59	12.25	

Fig. 18. The schematic diagram of the pigment synthesis via a solid-gas method. "Reproduced from Ref. [74] with permission from Elsevier.

In addition to the dopant amount, the synthesis parameters also affect the properties of γ-Ce$_2$S$_3$ pigments. Wu et al. [76] synthesized Na$^+$-doped ultrafine γ-Ce$_2$S$_3$ micro-pigments using a low-temperature combustion method. In this method, metallic nitrates are mixed with a complexing agent (in this case EDTA), and a gel is obtained that ignites at a certain temperature. The final product is a porous ultrafine powder. According to the CIELab results, these researchers selected a fixed ratio of $n_{Na/Ce}$=0.2 for all samples to investigate the effect of various $n_{EDTA/Ce}$= 1, 1.5, 2, and 2.5 on the morphology, particle size, and chromaticity of the pigments. Fig. 21 indicates the FESEM

microstructural images of Na$^+$ doped γ-Ce$_2$S$_3$ pigments obtained with various amounts of EDTA. When $n_{EDTA/Ce}$=1–2, the samples became fluffier and more porous with more EDTA additions. However, a densification process was noticed in the samples with higher EDTA additions ($n_{EDTA/Ce}$ >2). Fig. 22 shows the results of chromaticity experiments of Na$^+$-doped γ-Ce$_2$S$_3$ pigments with various EDTA additions. The effect of $n_{EDTA/Ce}$ on the chromaticity of the obtained pigments was not as significant as the doping levels; however, it could not be neglected. The best chromaticity was seen in the sample with $n_{EDTA/Ce}$=2 (L*=33.43, a*=38.32, and b*=32.34). Wang et al. [77] synthesized Na$^+$ doped γ-Ce$_2$S$_3$ nano pigments using a commercial ceria nanopowder, sodium carbonate, and carbon disulfide at 600–800 °C. The pigments calcined at 600 °C were fused particles and the color was brown. When temperature increased the color shifted to yellowish red (L*=44.93, a*=32.40 and b*=48.3) at 700 °C and then to bright red (L*=39.07, a*=42.78 and b*=43.12) at 800 °C. The pigment
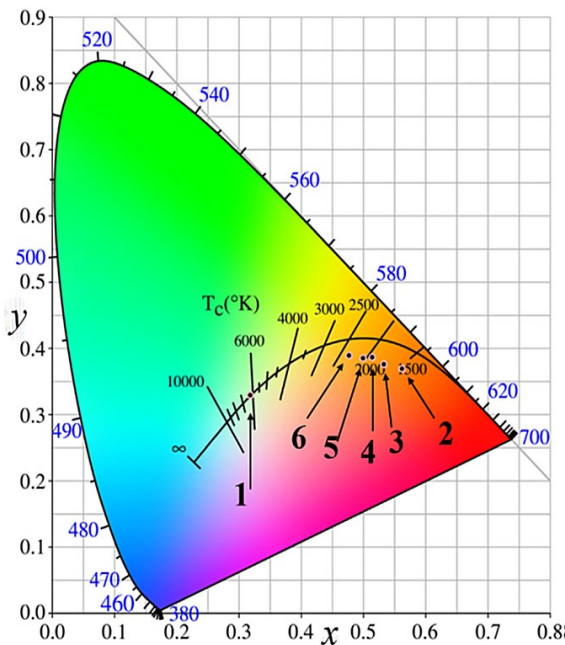

Fig. 19. Chromaticity values of γ-[K]-Ce$_2$S$_3$ with various amounts of dopant ($n_{K/Ce}$=0, 0.10, 0.15, 0.20, 0.25, and 0.30 corresponding to numbers 1, 2, 3, 4, 5, and 6, respectively). "Reproduced from Ref. [71] with permission from Elsevier. All rights reserved".

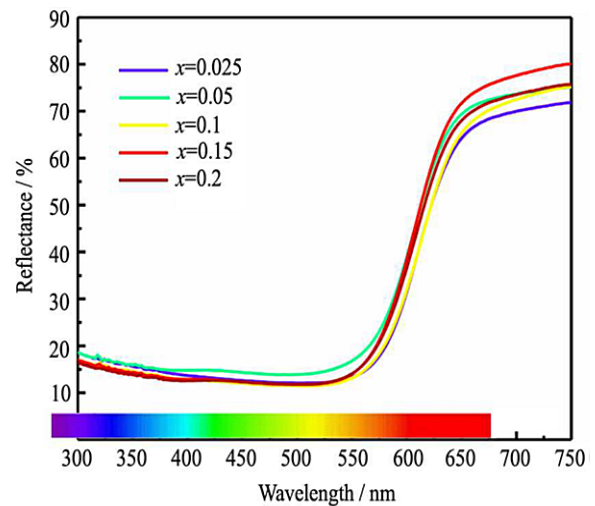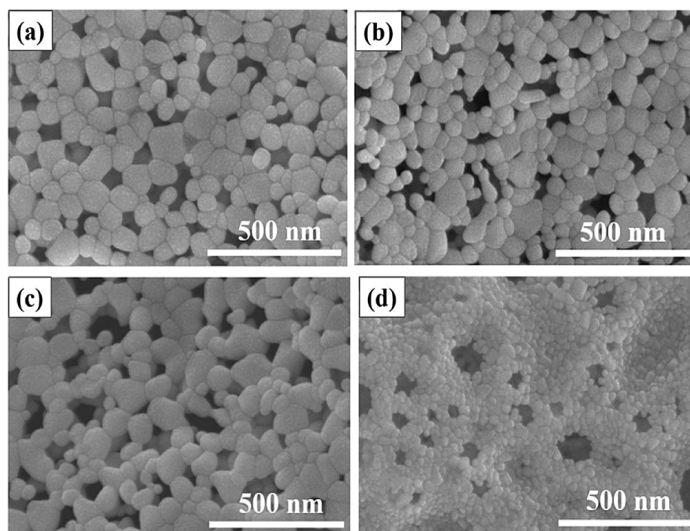
Fig. 20. UV-Vis reflectance spectra of Sr^{2+}, Dy^{3+}co-doped γ-Ce$_2$S$_3$ red pigments with various Dy^{3+}/Sr^{3+} ratios (x= 0.025–0.2). "Reproduced from Ref. [75] with permission from Elsevier. All rights reserved".
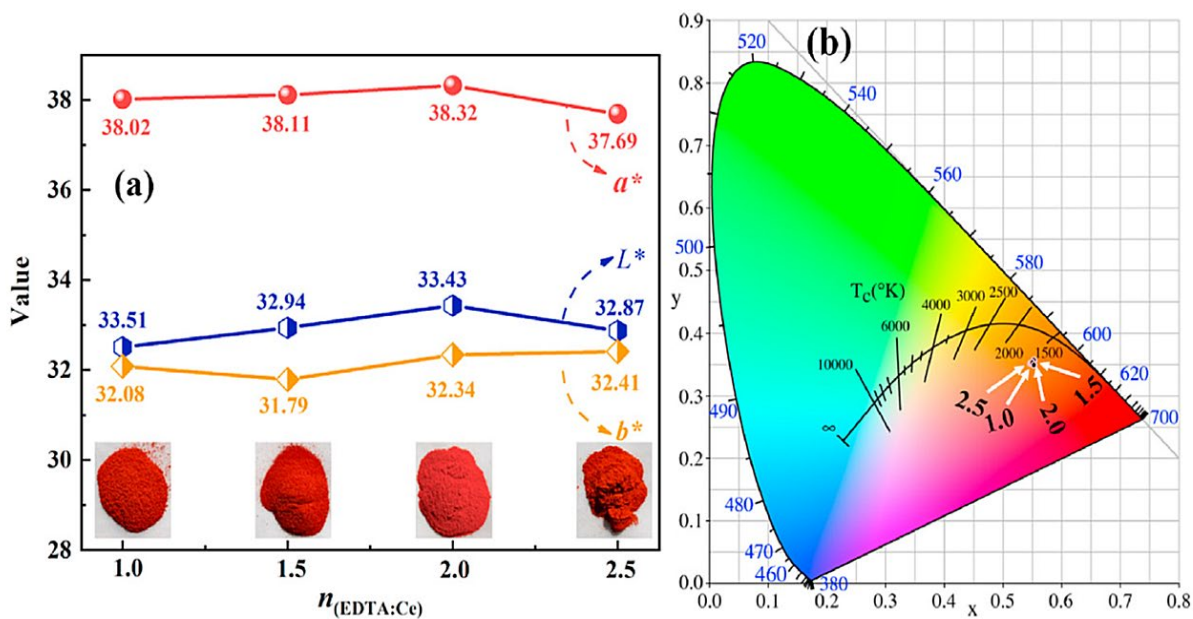
Fig. 21. FESEM images of the Na$^+$-doped γ-Ce$_2$S$_3$ pigments with various n$_{EDTA/Ce}$: a) 1, b) 1.5, c) 2.0, and d) 2.5. "Reproduced from Ref. [76] with permission from Elsevier. All rights reserved".

synthesized at 800 °C was considered the optimum sample and was applied in PVC and PE to examine the color performance. In another study, Yu et al. [78] investigated the effect of precursor size on the properties of Na$^+$ doped γ-Ce$_2$S$_3$ pigments (Na/Ce=0.2). Those authors synthesized ceria spheres with various particle sizes using a hydrothermal process. When the ceria sphere size was in the nanoscale, the γ-Ce$_2$S$_3$ phase was formed even at below 600 °C, but ceria micro pigments did not assist in the cerium trisulfide formation up to 800 °C. However, the bigger pigments had better thermal stabilities, while the smaller ones showed better color performance due to the better dispersibility of nanoparticles.

4.4.2. Core-shell γ-Ce$_2$O$_3$ pigments

The application of a surface coating is a beneficial method to improve the properties of core materials by contributions of the core and shell at the same time [79]. In an attempt to improve the thermal stability of γ-Ce$_2$S$_3$ pigments, Chen et al. [69] coated the pigments with SiO$_2$. The commercial Ce$_2$S$_3$ pigment was pretreated in multiple steps: (1) cleaning with sonication in acetone, ethanol, and distilled water twice, respectively; (2) drying under 50 °C, and (3) grinding in an agate mortar. The Stöber method was used to coat the pretreated pigment. In this method, the pigment was dispersed in ethanol and then magnetically and ultrasonically stirred for multiple times in separate

Fig. 22. a) Chromaticity and b) CIE color gamut coordinates of the Na$^+$-doped γ-Ce$_2$S$_3$ pigments with various n$_{EDTA/Ce}$. "Reproduced from Ref. [76] with permission from Elsevier. All rights reserved".
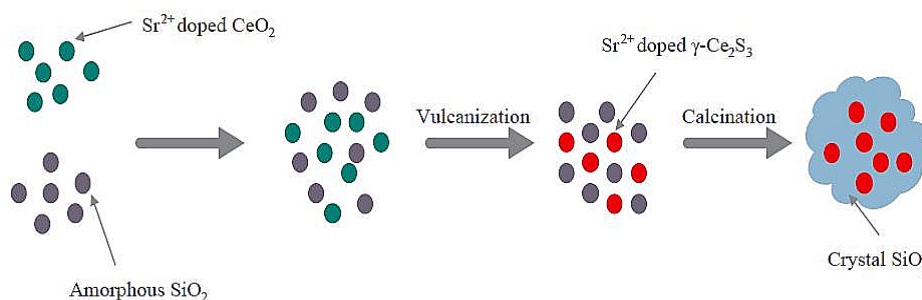
Fig. 23. A schematic illustration of the preparation process of Sr^{2+} doped γ-Ce₂S₃@c-SiO₂ pigments. "Reproduced from Ref. [80] with permission from Elsevier. All rights reserved".

steps. Then a solution made of THEOS and ethanol was added, and magnetic stirring continued for 20 min at 40 °C. After that, a solution of ammonia, ethanol, and distilled water was added, and stirring continued for 6 h. THEOS was hydrolyzed and SiO_2 was generated, forming a coating on the surface of pigments. The optimum cerium-to-silicon ratio was 2:1 for the best coating quality. The thermal stability of the pigment was expanded to 450 °C without any significant effect on the red color of the pigment. Although SiO_2 coating is useful for enhancing thermal stability, its low density is a limiting factor. So, aiming to overcome this barrier, Li et al. [80] coated Sr^{2+} doped γ-Ce₂S₃ particles with SiO_2 using the Stöber method and investigated the influences of the sulfurization temperature, the Ce^{3+}/Si^{4+} ratio, and the calcination temperature on the corrosion resistance, the chromaticity, and thermal stability of the pigments. The preparation process is schematically shown in Fig. 23. A better corrosion resistance and an improved coloring performance (L*=38.22, a*=28.97, and b*=25.49) were seen in the coated pigments with a Ce^{3+}/Si^{4+}=0.4. Application of the crystal SiO_2 coating enhanced the oxidation temperature of the γ-Ce₂S₃ pigments from 479 °C to 883 °C. In another study, Li et al. [81] prepared silica multi-coated γ-Ce₂S₃ micro-pigments using a sol-gel

method based on the Stöber route. The shell thicknesses of 70, 100, and 140 nm were obtained by repeating the coating process once, twice, and thrice (Figs. 24a–d). The thickest layer provided high thermal stability up to 570 °C and good chemical stability in a fritted glaze up to 620 °C (L*=30.28, a*=32.45, and b*=26.4). Song et al. [82] prepared pomegranate-like γ-[Li]-Ce₂S₃@c-SiO₂ (cristobalite) red core-shell micro-pigments (L*=39.15, a*=35.06, and b*=20.93) using a microemulsion method and controlled calcination with high chemical and thermal stabilities (after being soaked in the HCl for 24 and then being calcined at 900 °C in the air). In another study, Wu et al. [83] synthesized γ-Ce₂S₃@SiO₂ coated red pigments with a plum pudding mosaic structure and improved thermal stability (up to 900 °C) using a CeO₂@a-SiO₂ mesoporous precursor at a calcination temperature of 1300 °C and investigated the effect of pre-sintering temperature. The optimum pre-sintering temperature was 400 °C, giving the maximum surface area (274 m²/g), pore volume (0.27 cm³/g), and chromaticity (L*=30.46, a*=37.73, and b*=23.61).

For the first time, Mao et al. [79] synthesized core-shell Ce₂S₃@ZnO pigments to reduce the H₂S release during the production process and stated that a 40 nm ZnO surface could fully protect the core (L*=42.57,
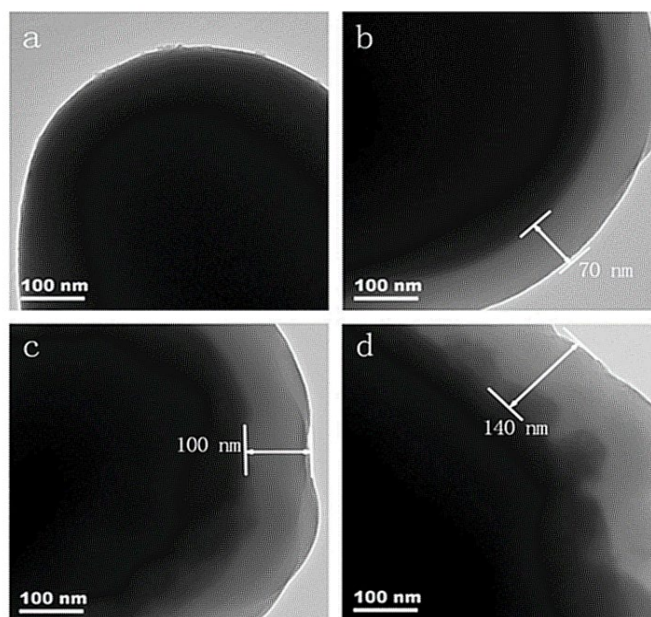
Fig. 24. TEM images of a) uncoated γ-Ce₂S₃ and b-d) multicoated γ-Ce₂S₃@SiO₂ micro-pigments. The coating process is repeated for a) 0, b) 1, c) 2, and d) 3 times. "Reproduced from Ref. [81] with permission from Elsevier. All rights reserved".
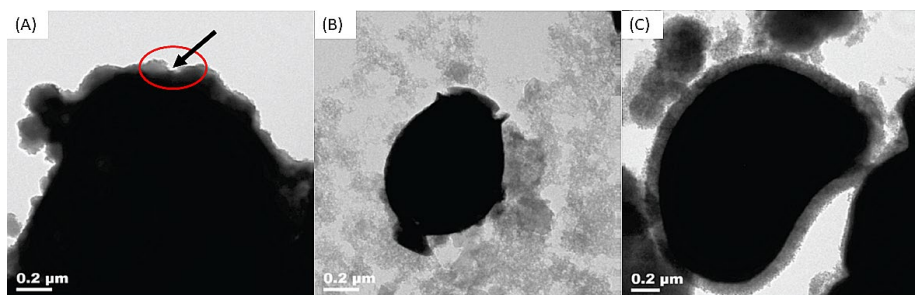
Fig. 25. TEM images of the γ-Ce$_2$S$_3$@ZrO$_2$ core-shell pigments obtained by a) the hydrolysis, b) the hydrothermal, and c) the combined methods. "Reproduced from Ref. [84] with permission from Trans Tech Publications, Ltd. All rights reserved".

a*=42.85, and b*=30.44), eliminate the H$_2$S release, and enhance thermal stability by maintaining the red color up to 380 °C. Gao et al. [84] synthesized γ-Ce$_2$S$_3$@ZrO$_2$ core-shell pigments using a combined hydrolysis-hydrothermal method at low temperatures. Figs. 25a–c show the TEM images of the core-shell pigments obtained by the hydrolysis, the hydrothermal, and the combined methods, respectively. The shell was not a uniform layer due to the zirconium n-butoxide hydrolysis (Fig. 25a). Many free ZrO$_2$ particles were seen due to their directional crystallization (Fig. 25b). Only Fig. 25c shows a uniform core-shell structure, attributed to the complete in-situ formation of a ZrO$_2$ layer with Zr-O-Zr bonds in the hydrolysis method, followed by fulfilling the layer by Zr^{4+} during the hydrothermal method. A 90 nm full layer was formed on the γ-Ce$_2$S$_3$ particles, maintaining its red color (L*=44.38, a*=31.94, b*=23.14) after heating up to 380 °C (L*=42.71, a*=26.23, b*=18.38).
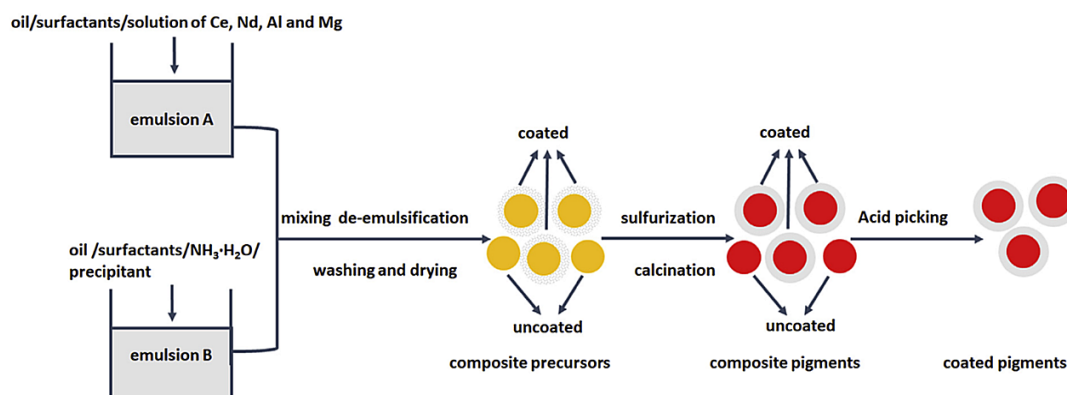
4.4.3. Composite pigments

Compositing is another method for optimizing the properties of γ-Ce$_2$S$_3$ red pigments. Zhang et al. [85] synthesized environmentally friendly mica/Ce$_{2-x}$Y$_x$S$_3$ composite pigments via the deposition of the sol-gel derived γ-Ce$_{2-x}$Y$_x$S$_3$ on mica. The results indicated the uniform particulate Ce$_{2-x}$YS$_3$ coating on mica. The doped pigments had one single pure gamma phase. The mica/γ-Ce$_{1.8}$Y$_{0.2}$S$_3$ could tolerate high temperatures up to 500 °C. This thermal stability was higher than both pure γ-Ce$_2$S$_3$ and the coated one. A shift to red-yellow was seen when yttrium was doped in the system. The a*, b*, and c* parameters

increased with yttrium additions, indicating a more red, more yellow, richer, and stronger color at the same time. These composite pigments showed excellent UV shielding ability, high NIR, and solar reflectance, widening their applications to cool materials, such as cool roofs. Li et al. [86] synthesized two kinds of aluminum-based (corundum and spinel) γ-Ce$_2$S$_3$ composite red pigments by sulfurization at 900 °C for 300 min and calcination of the microemulsion-derived precursors at 1200 °C for 60 min in an inert atmosphere and investigated the effect of sulfurization conditions on the phase composition. The applied materials for the precursor synthesis were cerium chloride, nitrates of neodymium, aluminum, and magnesium. B$_2$O$_3$ and CS$_2$ were used as the additive and the sulfur source. The synthesis process is schematically shown in Fig. 26. Aluminum-based composite pigments had both free and encapsulated γ-Ce$_2$S$_3$ materials. The former was removed using an acid-treatment and the latter was protected by the aluminum-based layer. This process slightly changed the color but improved thermal stability. The obtained γ-Ce$_2$S$_3$ spinel-based and corundum-based composite pigments had a bright red color (γ-Ce$_2$S$_3$-spinel: L=38.05, a*=34.27, and b*=30.59; γ-Ce$_2$S$_3$-corundum: L*=42.83, a*=34.22, and b*=30.59) and high thermal stabilities up to 474.5 °C and 479.5 °C, respectively. After the acid treatment, the pigments could maintain their red color up to 800 °C.

4.5. Red zircon pigments

Zircon (ZrSiO$_4$) pigments have been introduced before the 1970s. The zircon-based pigments are categorized based on the relationship

**Fig. 26.** A schematic illustrating the preparation process of aluminum-based (corundum and spinel) γ-Ce$_2$S$_3$ composite red pigments. "Reproduced from Ref. [86] with permission from Elsevier. All rights reserved".
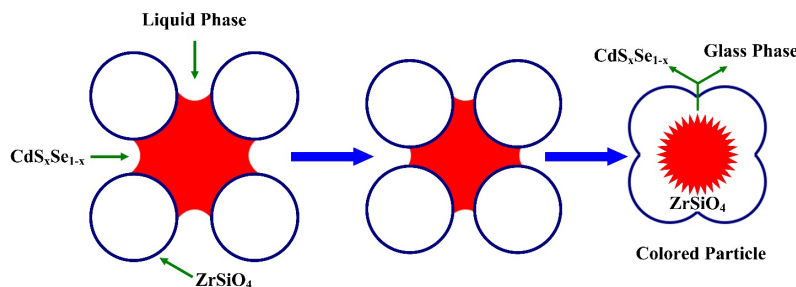
Fig. 27. A scheme of the cadmium sulphoselenide encapsulation process in zircon. "Redrawn from Ref. [28] with permission from Elsevier.

between the core (coloring materials) and the shell (or the encapsulating body) into the encapsulation and the ion-substituted pigments. The encapsulation pigments contain a compound in a zircon shell, but in the second case, the ion directly enters the zircon lattice [87]. A successful chromophore encapsulation requires synchronization between the shell crystallization/sintering and the core nucleation and growth, as their simultaneous occurrence is a necessity [9]. $CdS_xSe_{1-x}@ZrSiO_4$ [10, 88–91] and $Fe_2O_3@ZrSiO_4$ [91–98] are the known red zircon encapsulation pigments.

The toxicity and low thermal stability of the cadmium sulphoselenide pigments made way for the development of the $CdS_xSe_{1-x}@ZrSiO_4$ core-shell pigments. Zircon as a shell material with high thermal and chemical stabilities protects the cadmium sulphoselenide (the core). This inclusion process is schematically depicted in Fig. 27. Degussa company was the first to develop these pigments in the 1970s [89]. Ever since many researcher have tried to improve the properties of these pigments. Qin et al. [89] prepared submicron $CdS_xSe_{1-x}@ZrSiO_4$ inclusion pigments by the coprecipitation of Zr^{4+} and Si^{4+} ions on the silica shell of the $CdS_xSe_{1-x}@SiO_2$ pigments and using a PAAS surfactant for ink-jet applications. Thermal stability increased up to 1210 °C and the obtained pigments had a high-quality red color (L*=62.03, a*=27.35, and b*=19.64). Eftekhari Yekta et al. [90] synthesized cadmium sulphoselenide-zircon pigments using lithium fluoride as the mineralizer via a sol-gel method. The results showed that the zircon/CdS_xSe_{1-x} ratio had a determining role in the completion of the encapsulation process and an optimum ratio of 41 to 59 was reported. Unfortunately, no CIELab results were reported for the obtained pigments. However, the DRS results indicated a peak at 625 nm, consistent with the red wavelength. In a more recent study, Liu et al. [99] applied an integrated liquid approach for the preparation of $CdS_xSe_{1-x}@ZrSiO_4$ pigments for ink-jet applications. In this method, aqueous solutions of zirconium chloride/cadmium sulfate (A), sodium sulfide/sodium hydroxide/8selenium powder (B), monoethanolamine/hyper dispersant (C), sodium metasilicate (D), and the concentrated sulfuric acid (E) were prepared. At first solutions A and B, then D and E were added dropwisely to solution C while stirring. The obtained product was filtered, washed, and dried. Then it was crushed, mixed with lithium fluoride, and headed to the furnace for a heat treatment at 900 °C for 30min. The obtained powder was acid-soaked, washed, and dried in a vacuum at 60 °C for 12 h. The result was a wear-resistant strong bright red encapsulated pigment (L*=62.68, a*=30.66, and b*=22.54) with a uniform particle size distribution (200–1000 nm) and small spherical cores (20–100 nm), satisfying the ink-jet requirements.
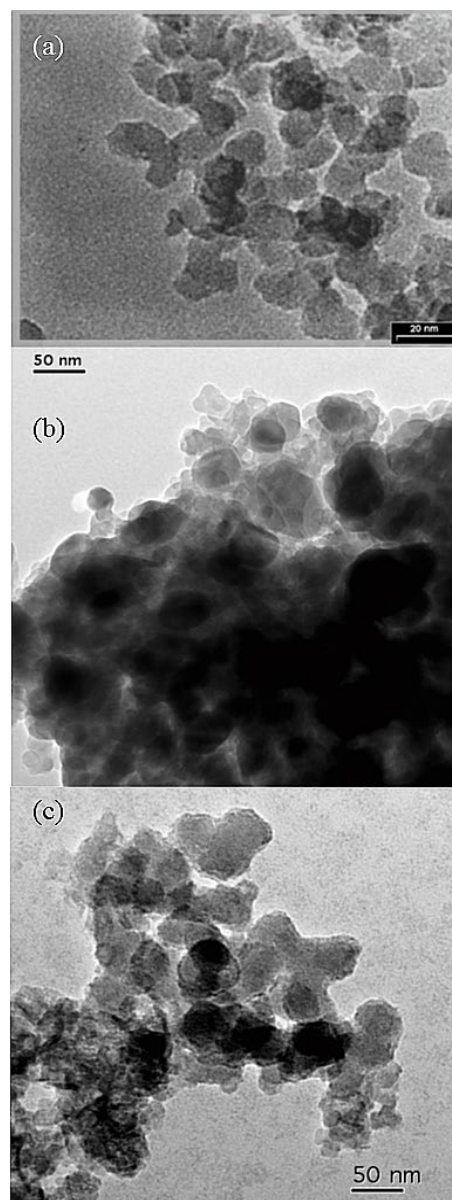
Fig. 28. TEM images of the synthesized red inclusion pigments: a) hematite-zircon-silica, b) hematite-zircon, and c) hematite-silica. "Reproduced from Ref. [94] with permission from Springer Nature.

Although hematite is an old nontoxic pigment, it does not show enough thermal and chemical stability at corrosive glazes and cannot give a stable shade alone. So it has to be encapsulated in more resistant shells, such as zircon and silica [93]. So, it has been attempted to develop these inclusion systems with high encapsulation efficiencies and lower costs in years. In a novel study, Andreola et al. [100] used rice husk ash as the silica source in the synthesis of hematite-zircon. The results showed that the rice husk ash contributed to a better encapsulation of hematite and a higher redness value due to a different crystallization/sintering rate for zircon. In a comparative study, Hosseini-zori [94] synthesized three inclusion red pigments (hematite-silica, hematite-zircon, and hematite-silica-zircon) using a sol-gel method, applied them in various glaze systems (alkalis, earth alkalis, leaded, and borate) and compared the colorimetric results and physical properties. Also, a commercial pigment based on the hematite-silica system was provided and applied in the glazes for comparison. The ternary nanocomposite pigments were obtained by substituting a part of zircon with cristobalite. The CIELab results of the synthesized pigments in various glaze systems are represented in Table 5. According to the colorimetric data, the highest redness value (a*=30.62) was obtained for the hematite-silica-zircon pigments in the earth-alkaline glaze. The hematite-silica pigment was only stable in the earth-alkaline glaze (the typical glaze for the monoprosa tiles) and had very different colors in other systems, showing insufficient thermal and chemical stabilities. The commercial pigment was unstable in all systems. But hematite-zircon and hematite-silica-zircon pigments showed red-orange and red-coral colors without any dissolution in the glaze systems, respectively. Figs. 28a–c show TEM images of the synthesized inclusion pigments. Nano hematite particles almost had the same size (5–10 nm) and spherical morphology in all inclusion systems. The author stated that the substitution of a fraction of zircon with silica would reduce the production color and also enhance the color intensity, resulting in a redder shade than the hematite-zircon pigment.

5. Discussion

Synthesis and application of red ceramic pigments have always been challenging due to the toxicity of the chromophores, and low thermal and chemical stabilities. Classic red pigments such as minium, cinnabar, realgar, and hematite have been used since ancient times. But they, excluding hematite, are highly toxic and forbidden in many countries. The lead-containing pigments can release metallic lead ions in water under the sunlight [31, 101] and pollute the aqueous environments. Minium pigments are capable of releasing their whole lead ions in water under UV radiation. Lead can accumulate in the brain, muscular, skeletal, and nervous systems and even affect the children's IQ [15]. The toxicity of cinnabar is lower than organic mercury, but the required mercury mining has a high risk of environmental pollution and exposure to toxic vapors [16]. Also, the mercury release from cinnabar has been reported [17]. The darkening process of cinnabar occurs mostly due to photo-induced reactions or interactions between the pigment and the binding media. The metallic mercury has been detected in the blackened cinnabar pigments [102]. Mercury is considered one of the top 10 chemicals with major public health concerns by WHO. As it can have toxic effects on the skin, lungs, eyes, kidneys, the immune, digestive, and nervous systems [16]. Although cadmium sulphoselenide pigments have not shown acute toxicity and are not water-soluble or skin-irritant, cadmium can be released in gastric acid. Cadmium ions can accumulate in the organs of animals and humans, specifically in the kidneys. Cadmium pigments are capable of polluting the environment, even in small amounts. Recycling these pigments requires special care and they should not be burned or dumped in nature [2]. Also, non-encapsulated cadmium pigments should not be consumed in the enameled drinking glasses; because the cadmium release is possible under the attack of acidic beverages [30]. The cadmium sulphoselenide pigments with higher CdSe amounts have shown more sensitivity to aggressive environments

Table 5. Chromaticity properties of the red glazes containing 5wt% inclusion pigments. E, L, A, and B stand for the earth alkalis, leaded, alkalis, and borate glazes, respectively. "Redrawn from Ref. [94] with permission from Springer Nature. All rights reserved".

Code of frit	color	L*	a*	b*	c*	h*
Hematite-silica pigment						
E	Red	39.92	26.59	18.40	32.33	34.60
L	Light red	45.21	27.49	18.80	33.30	34.36
A	Brown	39.26	13.99	11.87	18.35	40.33
B	Brown	41.60	11.51	9.23	14.76	38.72
Hematite-silica-zircon (ternary) pigment						
E	Red	39.46	30.62	23.61	38.67	37.63
L	Red	47.40	30.24	27.34	40.77	42.12
A	Red	45.83	27.45	19.58	33.72	35.50
B	Red (dark)	48.50	27.55	24.41	36.80	41.54
Hematite-zircon pigment						
E	Coral	33.13	17.65	9.92	20.25	29.34
L	Coral	36.79	16.67	10.67	19.80	32.63
A	Coral	33.56	14.82	8.45	17.06	29.69
B	Coral	34.03	17.55	9.54	19.98	28.52

[103]. Selenium is also capable of contaminating the aqueous environments and poisoning humans and animals [28]. In the case of lead chromate molybdate pigments, the molybdenum increases the release of toxic lead and chromium ions [25]. Arsenic which is the no. 1 toxic hazardous material constitutes 70% of realgar and is easily released under sunlight [23]. The mentioned toxic pigments are a few examples of industrially applied hazardous compounds. Preserving the environment is not an option, but a necessity. So, developing environmentally friendly alternatives for the mentioned hazardous pigments is inevitable. The alternatives should preferably show a pure red color with high chemical and thermal stabilities. Hematite is nontoxic, but unstable in the glazes and its red color is not divine. So, it is encapsulated to be protected from the harsh corrosive glazes and high temperatures [9, 93, 95, 104]. This method can also be applied to cadmium sulphoselenide pigments with an additional goal of reducing toxicity [29, 89]. Environmentally friendly inorganic red pigments include (but are not limited to) lanthanide-doped cerium oxides [61, 62] and perovskites [39, 49, 105–107], alkaline/earth-alkaline doped cerium trisulfides [74, 76], encapsulated zircon pigments [88, 90, 93, 96], iron oxide-based pigments [60, 92, 108–111]. Most of the studies were focused on obtaining intense red shades with high thermal and chemical stabilities. Although cadmium sulphoselenides are still the most beautiful red pigments with the highest redness values, the researchers have reached a milestone and some brilliant red pigments have already been commercialized.

6. Conclusions

Synthesis and applications of red inorganic pigments have been accompanied by various challenges and issues regarding the toxicity of the heavy elements for humans and the environment, low chemical and thermal stabilities, and high solar and atmospheric sensitivities. Many strategies have been applied to overcome these problems, including the toxic element entrapment by encapsulation, compositing, or its doping in stable structures to develop environmentally friendly alternatives such as cerium-based pigments or lanthanide-doped perovskites. Although none of the alternatives have reached the high redness value of the cadmium sulphoselenide pigments, researchers have reached a milestone in improving the red shade throughout several years of development. Researching for more stable environmentally friendly sustainable pigments with intense red shades must be continued to address the current environmental, health, industrial, and economic problems.

CRediT authorship contribution statement

Rayehe Tavakolipour: Conceptualization, Writing - original draft, Project administration, Investigation, Supervision, Validation.
Yueming Li: Writing – review & editing, Investigation, Resources.
Maryam Hosseini Zori: Writing – review & editing, Investigation, Resources.
Maria Ines Basso Bernardi: Writing – review & editing, Investigation, Resources.
Kun Li: Writing – review & editing, Investigation, Resources.
Aušra Čiuladienė: Writing – review & editing, Investigation, Resources.
Eva Miguel: Writing – review & editing, Investigation, Resources.

Data availability

The data underlying this article will be shared on reasonable request to the corresponding author.

Declaration of competing interest

The authors declare no competing interests.

Funding and acknowledgment

References

[1] B. Bae, N. Takeuchi, S. Tamura, N. Imanaka, Environmentally friendly orange pigments based on hexagonal perovskite-type compounds and their high NIR reflectivity, Dyes Pigm. 147 (2017) 523–528. https://doi.org/10.1016/j.dyepig.2017.08.015.

[2] G. Pfaff, Inorganic Pigments, 2nd ed., De Gruyter, Darmstadt. (2023). https://doi.org/10.1515/9783110743920.

[3] S. Divya, S. Das, New red pigments based on Li3AlMnO5 for NIR reflective cool coatings, Ceram. Int. 47 (2021) 30381–30390. https://doi.org/10.1016/j.ceramint.2021.07.218.

[4] D. Mićović, M.C. Pagnacco, P. Banković, J. Maletaškić, B. Matović, et al., The influence of short thermal treatment on structure, morphology and optical properties of Er and Pr doped ceria pigments: Comparative study, Proc. Appl. Ceram. 13 (2019) 310–321. https://doi.org/10.2298/PAC1903310M.

[5] V. James, P. Prabhakar Rao, S. Sameera, S. Divya, Multiferroic based reddish brown pigments: Bi1-xM xFeO3 (M=Y and La) for coloring applications, Ceram. Int. 40 (2014) 2229–2235. https://doi.org/10.1016/j.ceramint.2013.07.141.

[6] E.B. Faulkner, R.J. Schwartz, High performance pigments, Wiley-VCH. (2009).

[7] H. Hashimoto, J. Kiyohara, A. Isozaki, Y. Arakawa, T. Fujii, et al., Bright Yellowish-Red Pigment Based on Hematite/Alumina Composites with a Unique Porous Disk-like Structure, ACS Omega. 5 (2020) 4330–4337. https://doi.org/10.1021/acsomega.9b04297.

[8] O. Opuchovic, G. Kreiza, J. Senvaitiene, K. Kazlauskas, A. Beganskiene, A. Kareiva, Sol-gel synthesis, characterization and application of selected sub-microsized lanthanide (Ce, Pr, Nd, Tb) ferrites, Dyes Pigm. 118 (2015) 176–182. https://doi.org/10.1016/j.dyepig.2015.03.017.

[9] M. Hosseini-Zori, E. Taheri-Nassaj, A.R. Mirhabibi, Effective factors on synthesis of the hematite-silica red inclusion pigment, Ceram. Int. 34 (2008) 491–496. https://doi.org/10.1016/j.ceramint.2006.11.012.

[10] H.F. Liu, W.B. Dai, H. Wang, L.K. Zeng, Y.M. Wang, Study on the preparation of the CdSxSe1−x@ZrSiO4 red ceramic pigments and its properties, J. Solgel Sci. Technol .75 (2015) 198–205. https://doi.org/10.1007/s10971-015-3689-1.

[11] C. Molinari, S. Conte, C. Zanelli, M. Ardit, G. Cruciani, M. Dondi, Ceramic pigments and dyes beyond the inkjet revolution: From technological requirements to constraints in colorant design, Ceram. Int. 46 (2020) 21839–21872. https://doi.org/10.1016/j.ceramint.2020.05.302.

[12] A. Amat, F. Rosi, C. Miliani, P. Sassi, M. Paolantoni, S. Fantacci, A combined theoretical and experimental investigation of the electronic and vibrational properties of red lead pigment, J. Cult. Herit. 46 (2020) 374–381. https://doi.org/10.1016/j.culher.2020.04.014.

[13] A. Abel, The history of dyes and pigments, Colour Design, Elsevier. (2012) 557–587. https://doi.org/10.1016/b978-0-08-101270-3.00024-2.

[14] E. Gliozzo, C. Ionescu, Pigments—Lead-based whites, reds, yellows and oranges and their alteration phases, Archaeol. Anthropol. Sci. 14 (2022) 17. https://doi.org/10.1007/s12520-021-01407-z.

[15] Z. She, M. Yang, T. Luo, X. Feng, J. Wei, X. Hu, Lead release and species transformation of commercial minium pigments in aqueous phase under UV-irradiation, Chemosphere. 269 (2021) 128769. https://doi.org/10.1016/j.chemosphere.2020.128769.

[16] E. Gliozzo, Pigments — Mercury-based red (cinnabar-vermilion) and white (calomel) and their degradation products, Archaeol. Anthropol. Sci. 13 (2021) 210. https://doi.org/10.1007/s12520-021-01402-4.

[17] R. Nöller, Cinnabar reviewed: Characterization of the red pigment and its reactions, Stud. Conserv. 60 (2015) 79–87. https://doi.org/10.1179/2047058413Y.0000000089.

[18] E. Gliozzo, L. Burgio, Pigments—Arsenic-based yellows and reds, Archaeol. Anthropol. Sci. 14 (2022) 4. https://doi.org/10.1007/s12520-021-01431-z.

[19] A. Čiuladienė, A. Kareiva, R. Raudonis, From model to artefact: Versatile characterization of cinnabar, red lead and realgar red paints for rubrics and miniatures, Chemija. 31 (2020) 238–246.

[20] S.J.S. Flora, Arsenic: Chemistry, Occurrence, and Exposure, Handbook of Arsenic Toxicology, Elsevier Inc. (2015) 1–49. https://doi.org/10.1016/B978-0-12-418688-0.00001-0.

[21] I.D. Rae, Arsenic: its chemistry, its occurrence in the earth and its release into industry and the environment, ChemTexts. 6 (2020) 25. https://doi.org/10.1007/s40828-020-00118-7.

[22] V.M. Nurchi, A.B. Djordjevic, G. Crisponi, J. Alexander, G. Bjørklund, J. Aaseth, Arsenic toxicity: Molecular targets and therapeutic agents, Biomolecules. 10 (2020) 235. https://doi.org/10.3390/biom10020235.

[23] L. Liu, Z. Zhang, M. Zhang, X. Yang, C. Liu, G. Qiu, Mechanism of arsenic release from realgar oxidation in the presence of dissolved oxygen: Effect of reactive oxygen species and light-induced transformation, Geochim. Cosmochim. Acta. 339 (2022) 58–69. https://doi.org/10.1016/j.gca.2022.10.037.

[24] A. Čiuladienė, A. Luckutė, J. Kiuberis, A. Kareiva, Investigation of the chemical composition of red pigments and binding media, Chemija. 29 (2018) 243–256. https://doi.org/10.6001/chemija.v29i4.3840.

[25] H. Liu, S. Zhang, X. Qu, H. Fu, L. Zuo, Molybdenum doping leads to faster photo-dissolution of 2 commercial Molybdate Red pigment than chrome yellow 3 pigment under sunlight irradiation, SSRN. (2024). https://doi.org/https://dx.doi.org/10.2139/ssrn.4880639.

[26] L. Erkens, H. Hamers, R. Hermans, E. Claeys, M. Bijnens, Lead chromates: A review of the state of the art in 2000, Surf. Coat. Int. B: Coat. Trans. 84 (2001) 169–176. https://doi.org/10.1007/BF02700395.

[27] Y. Marinova, J.M. Hohemberger, E. Cordoncillo, P. Escribano, J.B. Carda, Study of solid solutions, with perovskite structure, for application in the field of the ceramic pigments, J. Eur. Ceram. Soc. 23 (2003) 213–220. https://doi.org/10.1016/S0955-2219(02)00182-6.

[28] J. Wu, K. Li, X. Xu, Y. Zhang, X. Xu, X. Lao, Research and development of cadmium sulphoselenide red pigment, J. Wuhan Univ. Technol. Mater. Sci. Ed. 30 (2015) 1247–1254. https://doi.org/10.1007/s11595-015-1303-6.

[29] J. Wu, K. Li, X. Xu, J. Yu, X. Li, J. Tian, In situ synthesis of spherical CdS1-xSex red pigment used for ceramic ink-jet printing, Mater. Chem. Phys. 203 (2018) 193–201. https://doi.org/10.1016/j.matchemphys.2017.09.070.

[30] A. Turner, Cadmium pigments in consumer products and their health risks, Sci. Total Environ. 657 (2019) 1409–1418. https://doi.org/10.1016/j.scitotenv.2018.12.096.

[31] H. Liu, K. Liu, H. Fu, R. Ji, X. Qu, Sunlight mediated cadmium release from colored microplastics containing cadmium pigment in

aqueous phase, Environ. Pollut. 263 (2020) 114484. https://doi.org/10.1016/j.envpol.2020.114484.

[32] K. Li, Q. Luo, R. Bai, Y. Li, C. Tang, et al., Synthesis and Characterization of Hydrothermal Synthesized Ultra-Red CdS1−xSe x Pigment, Trans. Indian Ceram. Soc. 82 (2023) 259–264. https://doi.org/10.1080/0371750X.2023.2236658.

[33] Y. Chen, X. Ren, K. Zhang, L. Wang, Structure and optical property of CdS1−xSex/CdS nanocomposite prepared by a simple and low cost approach, Mater. Sci. Eng: B. 243 (2019) 183–188. https://doi.org/10.1016/j.mseb.2019.04.011.

[34] C.A. Vanderhyde, S.D. Sartale, J.M. Patil, K.P. Ghoderao, J.P. Sawant, R.B. Kale, Room temperature chemical bath deposition of cadmium selenide, cadmium sulfide and cadmium sulfoselenide thin films with novel nanostructures, Solid State Sci. 48 (2015) 186–192. https://doi.org/10.1016/j.solidstatesciences.2015.08.007.

[35] Y. Chen, Y. Ou-Yang, A novel approach to the synthesis of CdS1-xSex solid solution at room temperature, Mater. Sci. Eng: B. 142 (2007) 112–115. https://doi.org/10.1016/j.mseb.2007.06.013.

[36] Y. Chen, C. Li, X. Ren, K. Zhang, L. Wang, Photoluminescence and Crystallinity of High Quality CdS1−xSex Synthesized in Ammonium Water Medium, J. Electron. Mater. 50 (2021) 4145–4154. https://doi.org/10.1007/s11664-021-08953-1.

[37] K.V. Khot, S.S. Mali, N.B. Pawar, R.R. Kharade, R.M. Mane, et al., Simplistic construction of cadmium sulfoselenide thin films via a hybrid chemical process for enhanced photoelectrochemical performance, RSC Adv. 5 (2015) 40283–40296. https://doi.org/10.1039/c4ra16311g.

[38] M. Ardit, G. Cruciani, M. Dondi, C. Zanelli, Pigments Based on Perovskite, Perovskites and Related Mixed Oxides, Wiley. (2016) 259–288. https://doi.org/10.1002/9783527686605.ch12.

[39] G. Baldi, N. Dolen, A. Barzanti, V. Faso, Synthesis of a New Class of Red Pigments Based on Perovskite - Type Lattice AxB(2-x-y)CryO3 with 0.90<x<1, 1 0.05<y<0.12 A = Y, lanthanides, B= Al for use in body stain and high temperature glazes, Key Eng. Mater. 264–268 (2004) 1545–1548. https://doi.org/10.4028/www.scientific.net/KEM.264-268.1545.

[40] M. Jansen, H.P. Letschert, Inorganic Yellow-Red Pigments Without Toxic Metals, Nature. 404 (2000) 980–982. https://doi.org/10.1038/35010082.

[41] C. Gargori, R. Galindo, M. Llusar, S. Cerro, A. García, G. Monrós, New Chromium-Calcium Titanate Red Ceramic Pigment, Adv. Sci. Technol. 68 (2010) 208–212. https://doi.org/10.4028/www.scientific.net/AST.68.208.

[42] F. Matteucci, M. Dondi, G. Cruciani, G. Baldi, A. Barzanti, Colouring mechanism of red ceramic pigments based on perovskite structure, Key Eng. Mater. 264–268 (2004) 1549–1552. https://doi.org/10.4028/www.scientific.net/kem.264-268.1549.

[43] M. Shirpour, M.A.F. Sani, A. Mirhabibi, Synthesis and study of a new class of red pigments based on perovskite YAlO3 structure, Ceram. Int. 33 (2007) 1427–1433. https://doi.org/10.1016/j.ceramint.2006.04.023.

[44] S. Ahmadi, A. Aghaei, B.E. Yekta, Effective parameters for synthesis of chromium doped YAlO3 red pigment, Pigm. Resin Technol. 44 (2015) 1–6. https://doi.org/10.1108/PRT-02-2014-0013.

[45] G.N. Marques, T.P. Oliveira, M.M. Teixeira, A.V. Lot, M.F. do Nascimento, et al., Synthesis of yttrium aluminate doped with Cr3+ using MgF2–Na2B4O7 as mineralizers to obtain red pigments for ceramic tiles application, Ceram. Int. 46 (2020) 27940–27950. https://doi.org/10.1016/j.ceramint.2020.07.287.

[46] E. Miguel, G. Paulo-Redondo, J.B. Carda Castelló, I. Nebot-Díaz, Comparative Study of the Synthesis of a Red Ceramic Pigment Using Microwave Heat Treatment, Colorants. 2 (2023) 518–532. https://doi.org/10.3390/colorants2030025.

[47] S. Blasco-Zarzoso, H. Beltrán-Mir, E. Cordoncillo, Sustainable inorganic pigments with high near-infra-red reflectance based on Fe3+ doped YAlO3 for high temperature applications, J. Alloys

Compd. 960 (2023) 170695.
https://doi.org/10.1016/j.jallcom.2023.170695.

[48] K. Yamaguchi, Y. Shobu, R. Oka, T. Masui, Color Controllable Inorganic Pigments with Ce3+ as a Color Source, Inorg. Chem. 62 (2023) 15392–15402.
https://doi.org/10.1021/acs.inorgchem.3c01292.

[49] E. Miguel, J.B. Carda Castelló, I. Nebot-Díaz, Development of Red Ceramic Pigments with Perovskite Structure Prepared through a Traditional Route, Eng. 4 (2023) 159–173.
https://doi.org/10.3390/eng4010010.

[50] Y. Chen, J. Zou, Cr and Mg co-doped YAlO3 red cool pigments with high NIR reflectance and infrared emissivity for sustainable energy-saving applications, Ceram. Int. 49 (2023) 13717–13727.
https://doi.org/10.1016/j.ceramint.2022.12.250.

[51] Y. Chen, J. Zou, H. Lin, P. Zhang, Enhancing colour and solar reflective performances for Cr-doped YAlO3 red pigment by tailoring chemical defects with the aid of CaCO3 and Na2B4O7 mineralizers, J. Alloys Compd. 932 (2023) 167652.
https://doi.org/10.1016/j.jallcom.2022.167652.

[52] M. Fortuño-Morte, P. Serna-Gallén, H. Beltrán-Mir, E. Cordoncillo, A new series of environment-friendly reddish inorganic pigments based on AFeO3 (A = Ln, Y) with high NIR solar reflectance, J. Materiomics. 7 (2021) 1061–1073.
https://doi.org/10.1016/j.jmat.2021.02.002.

[53] M. Fortuño-Morte, P. Serna-Gallén, H. Beltrán-Mir, E. Cordoncillo, The influence of Ca2+ and Zn2+ doping on the development of sustainable pigments based on GdFeO3 perovskite: From a reddish colour towards a pure black, Ceram. Int. 48 (2022) 21469–21478.
https://doi.org/10.1016/j.ceramint.2022.04.111.

[54] A. Čiuladienė, A. Beganskienė, J. Senvaitienė, A. Kareiva, Study of the red iron paints for rubrics and miniatures: Accelerated aging and analytical data, Medziagotyra. 27 (2021) 77–83.
https://doi.org/10.5755/j02.ms.25190.

[55] N. Mufti, T. Atma, A. Fuad, E. Sutadji, Synthesis and characterization of black, red and yellow nanoparticles pigments from the iron sand, AIP Conf Proc, American Institute of Physics Inc. (2014) 165–169. https://doi.org/10.1063/1.4897129.

[56] H. Hashimoto, K. Higuchi, H. Inada, Y. Okazaki, T. Takaishi, H. Asoh, Well-Dispersed α-Fe2O3 Particles for Lead-Free Red Overglaze Enamels through Hydrothermal Treatment, ACS Omega. 1 (2016) 9–13. https://doi.org/10.1021/acsomega.6b00040.

[57].R.A. Candeia, M.I.B. Bernardi, E. Longo, I.M.G. Santos, A.G. Souza, Synthesis and characterization of spinel pigment CaFe2O 4 obtained by the polymeric precursor method, Mater. Lett. 58 (2004) 569–572.
https://doi.org/10.1016/S0167-577X(03)00563-9.

[58] Y. Lu, W. Dong, W. Wang, J. Ding, Q. Wang, et al., Optimal synthesis of environment-friendly iron red pigment from natural nanostructured clay minerals, Nanomaterials. 8 (2018) 925.
https://doi.org/10.3390/nano8110925.

[59] M. Quddus, M. Rahman, J. Khanam, B. Biswas, N. Sharmin, et al., Synthesis and Characterization of Pigment Grade Red Iron Oxide from Mill Scale, Int. Res. J. Pure Appl. Chem. 16 (2018) 1–9.
https://doi.org/10.9734/irjpac/2018/42935.

[60] T.E.R. Fiuza, J.F.M. Borges, J.B.M. da Cunha, S.R.M. Antunes, A.V.C. de Andrade, et al., Iron-based inorganic pigments from residue: Preparation and application in ceramic, polymer, and paint, Dyes Pigm. 148 (2018) 319–328.
https://doi.org/10.1016/j.dyepig.2017.09.025.

[61] I. Nurhasanah, Y. Astuti, P. Triadiyaksa, Precipitation Synthesis of CeO2 Nanopowder Pigment, J. Rekayasa Kim. Lingkung. 18 (2023) 29–36. https://doi.org/10.23955/rkl.v18i1.28648.

[62] L.A. Gonzaga, V.T. Santana, M.I.B. Bernardi, J. Hrubý, P. Neugebauer, A. Mesquita, CeO2 and CeO2:Pr nanocrystalline powders prepared by the polymeric precursor method: Yellow and red pigments with tunable color, J. Am. Ceram. Soc. 103 (2020) 6280–6288. https://doi.org/10.1111/jace.17339.

[63] L.S. Kumari, P.P. Rao, S. Sameera, P. Koshy, Synthesis and optical properties of Ce 0.95Pr 0.05-xM xO 2 (M = Mn, Si) as potential ecological red pigments for coloration of plastics, Ceram. Int. 38 (2012) 4009–4016. https://doi.org/10.1016/j.ceramint.2012.01.057.

[64] S. Radhika, K.J. Sreeram, B. Unni Nair, Effective synthesis route for red-brown pigments based on Ce-Pr-Fe-O and their potential application for near infrared reflective surface coating, J. Chem. Sci. 126 (2014) 65–73. https://doi.org/10.1007/s12039-013-0559-7.

[65] S.T. Aruna, S. Ghosh, K.C. Patil, Combustion synthesis and properties of Ce1−xPrxO2−δ red ceramic pigments, Int. J. Inorg. Mater. 3 (2001) 387–392. https://doi.org/10.1016/S1466-6049(01)00020-4.

[66] M. Llusar, L. Vitásková, P. Šulcová, M.A. Tena, J.A. Badenes, G. Monrós, Red ceramic pigments of terbium-doped ceria prepared through classical and non-conventional coprecipitation routes, J. Eur. Ceram. Soc. 30 (2010) 37–52.
https://doi.org/10.1016/j.jeurceramsoc.2009.08.005.

[67] Y. Li, X. Li, Z. Li, Z. Wang, Y. Hong, F. Song, Preparation, characterization, and properties of a Ba2+–Sm3+ co-doped γ-Ce2S3 red pigment, Solid State Sci. 106 (2020) 106332.
https://doi.org/10.1016/j.solidstatesciences.2020.106332.

[68] R.M.A. Khalil, M.I. Hussain, M. Imran, F. Hussain, N. Saeed, et al., First-principles simulation of structural, electronic and optical properties of cerium trisulfide (Ce2S3) compound, J. Electron. Mater. 50 (2021) 1637–1643. https://doi.org/10.1007/s11664-020-08478-z.

[69] G. Chen, Z. Zhu, H. Liu, Y. Wu, C. Zhu, Preparation of SiO2 coated Ce2S3 red pigment with improved thermal stability, J. Rare Earths. 31 (2013) 891–896. https://doi.org/10.1016/S1002-0721(12)60375-5.

[70] Y.Q. Gao, Y.M. Li, Z.M. Wang, Z.Y. Shen, Z.X. Xie, Preparations and characterizations of γ-Ce2S3 red pigments from Pr-doped CeO2 with improved thermal stabilities, Appl. Phys. A: Mater. Sci. Proc. 124 (2018) 151. https://doi.org/10.1007/s00339-018-1588-3.

[71] X. Li, Y. Li, F. Song, Z. Wang, Y. Hong, Z. Li, Study of K+ doping on structure and properties of γ-Ce2S3, J. Rare Earths. 38 (2020) 776–783. https://doi.org/10.1016/j.jre.2019.05.007.

[72] X. Li, Y.M. Li, Z.M. Wang, Y. Hong, Z.K. Li, Influence of Ba2+ doping on the properties and thermal stability of γ-Ce2S3, Appl. Phys. A: Mater. Sci. Proc. 125 (2019) 518.
https://doi.org/10.1007/s00339-019-2798-z.

[73] X. Li, Y. Li, Z. Li, Z. Wang, Y. Hong, F. Song, Preparation and properties of Ba2+-Y3+ co-doped gamma-Ce2S3 red pigment, Mater. Ceram. 71 (2019) 378–388.

[74] F. Song, Y. Li, Y. Yu, Z. Shen, Z. Wang, X. Li, Engineering the crystal structure of γ-[Li]-Ce2S3 red pigments for enhanced thermal stability, J. Solid State Chem. 282 (2020) 121110.
https://doi.org/10.1016/j.jssc.2019.121110.

[75] Y. Li, Q. Liu, F. Song, Z. Wang, Z. Shen, Y. Hong, Effect of Sr2+ and Dy3+ co-doping on coloration and temperature stabilization of a γ-Ce2S3 red pigment, J. Rare Earths. 38 (2020) 213–218.
https://doi.org/10.1016/j.jre.2019.02.015.

[76] F. Wu, X. Li, Y. Li, F. Song, Z. Wang, Z. Shen, Low-temperature combustion synthesis method to prepare Na+-doped ultrafine micron-sized γ-Ce2S3 bright red pigments, J Solid State Chem. 299 (2021) 122146. https://doi.org/10.1016/j.jssc.2021.122146.

[77] D. Wang, Y. Zhao, S. Yu, Synthesis of γ-Ce2S3 colorant under low temperature and its coloring properties for PE and PVC, J. Rare Earths. 35 (2017) 1042–1046. https://doi.org/10.1016/S1002-0721(17)61011-1.

[78] S. Yu, D. Wang, X. Gao, H. Su, Effects of the precursor size on the morphologies and properties of γ-Ce2S3 as a pigment, J. Rare Earths. 32 (2014) 540–544. https://doi.org/10.1016/S1002-0721(14)60105-8.

[79] W.-X. Mao, W. Zhang, Z.-X. Chi, R.-W. Lu, A.-M. Cao, L.-J. Wan, Core–shell structured Ce2S3 @ZnO and its potential as a pigment, J. Mater. Chem. A: Mater. 3 (2015) 2176–2180.
https://doi.org/10.1039/C4TA05797J.

[80] Y. Li, S. Le, Z. Wang, Y. Hong, K. Li, Q. Pu, Preparation and characterization of the Sr2+-doped γ-Ce2S3@c-SiO2 red pigments

exhibiting improved temperature and acid stability, Appl. Surf. Sci. 508 (2020) 145266. https://doi.org/10.1016/j.apsusc.2020.145266.

[81] Y.M. Li, S.G. Liu, F.S. Song, Z.M. Wang, Z.Y. Shen, Z.X. Xie, Preparation and thermal stability of silica layer multicoated γ-Ce2S3 red pigment microparticles, Surf. Coat. Technol. 345 (2018) 70–75. https://doi.org/10.1016/j.surfcoat.2018.04.023.

[82] F. Song, Y. Li, Y. Yu, Z. Shen, Z. Wang, In situ construction of pomegranate-like γ-[Li]-Ce2S3@ c-SiO2 as high-temperature and acid tolerant red pigment, Appl. Surf. Sci. 554 (2021) 149643. https://doi.org/10.1016/j.apsusc.2021.149643.

[83] F. Wu, X. Li, Y. Li, Z. Wang, Y. Hong, et al., Design and preparation of a type of γ-Ce2S3@c-SiO2-coated red pigment with a plum pudding mosaic structure: The effect of pre-sintering temperature on pigment properties, Microporous Mesoporous Mater. 311 (2021). https://doi.org/10.1016/j.micromeso.2020.110699.

[84] Y.Q. Gao, Y.M. Li, Z.M. Wang, Z.Y. Shen, Z.X. Xie, Preparation of γ-Ce2S3@ZrO2 red pigment by hydrolysis combined hydrothermal two steps method, Key Eng. Mater. 768 (2018) 172–178. https://doi.org/10.4028/www.scientific.net/KEM.768.172.

[85] S. Zhang, M. Ye, S. Chen, A. Han, Y. Zang, Synthesis and characterization of mica/γ-Ce2−xYxS3 composite red pigments with UV absorption and high NIR reflectance, Ceram. Int. 42 (2016) 16023–16030. https://doi.org/10.1016/j.ceramint.2016.07.111.

[86] Y. Li, Y. Gao, Z. Wang, Z. Shen, Y. Hong, F. Song, Synthesis and characterization of aluminum-based γ-Ce2S3 composite red pigments by microemulsion method, J. Alloys Compd. 812 (2020) 152100. https://doi.org/10.1016/j.jallcom.2019.152100.

[87] B. Lei, W. Qin, G. Kang, C. Peng, J. Wu, Modeling and evaluation for encapsulation efficiency of zircon-based heteromorphic encapsulation pigments, Dyes Pigm. 112 (2015) 245–254. https://doi.org/10.1016/j.dyepig.2014.07.010.

[88] J.M. Rincón, Pigment zircon-cadmium for ceramics, Conference: SECV, Trans. J. Br. Ceram. Soc. (1981)

[89] W. Qin, K. Wang, Y. Zhang, Preparation of submicron CdSxSe1-x@ZrSiO4 inclusion pigment and its application in ink-jet printing, J. Eur. Ceram. Soc. 41 (2021) 7878–7885. https://doi.org/10.1016/j.jeurceramsoc.2021.08.008.

[90] B.E. Yekta, M. Tamizifar, N. Rahimi, Synthesis of a Zircon-Cadmium Sulfo Selenide Pigment by a Sol-Gel Technique, J. Ceram. Soc. Jpn. 115 (2007) 757–760. https://doi.org/10.2109/jcersj2.115.757.

[91] F. Zhao, Y. Gao, H. Luo, Reactive formation of Zircon inclusion pigments by deposition and subsequent annealing of a Zirconia and silica double shell, Langmuir. 25 (2009) 13295–13297. https://doi.org/10.1021/la903197t.

[92] E. Zumaquero, M.J. Orts, V. Sanz, S. Mestre, Iron zircon pigment synthesis: Proposal of a mixing index for the raw materials mixtures, Bol. Soc. Esp. Ceram. Vidr. 56 (2017) 177–185. https://doi.org/10.1016/j.bsecv.2017.01.003.

[93] H. Heydari, R. Naghizadeh, H.R. samimbanihashemi, M. Hosseini Zori, Synthesis and characterisation of hematite-zircon nanocomposite by sol - Gel method, Adv. Mat. Res. 829 (2014) 544–548. https://doi.org/10.4028/www.scientific.net/AMR.829.544.

[94] M. Hosseini-Zori, Substitution of a fraction of zircon by cristobalite in nano hematite encapsulated pigment and examination of glaze application, J. Adv. Ceram. 2 (2013) 149–156. https://doi.org/10.1007/s40145-013-0054-0.

[95] M. Hosseini-Zori, Microstructure of nanoscale hematite encapsulated by zircon and cristobalite in ceramic pigment and examination of glazes application, J. Adv. Microsc. Res. 8 (2013) 61–66. https://doi.org/10.1166/jamr.2013.1138.

[96] Y. Wang, Q. Wang, Q. Chang, Y. Wang, Y. Zhao, et al., Chromatic study on the coloration mechanism of iron zircon pigment, Mater.

Chem. Phys. 235 (2019) 121740. https://doi.org/10.1016/j.matchemphys.2019.121740.

[97] L.M. Schabbach, F. Bondioli, M.C. Fredel, Color prediction with simplified Kubelka-Munk model in glazes containing Fe2O3-ZrSiO4 coral pink pigments, Dyes Pigm. 99 (2013) 1029–1035. https://doi.org/10.1016/j.dyepig.2013.08.009.

[98] M. Cannio, F. Bondioli, Mechanical activation of raw materials in the synthesis of Fe2O3-ZrSiO4 inclusion pigment, J. Eur. Ceram. Soc. 32 (2012) 643–647. https://doi.org/10.1016/j.jeurceramsoc.2011.10.008.

[99] H. Liu, X. Zeng, X. Zhang, R. Liu, W. Liu, et al. An Integrated Liquid Approach To The Synthesis of CdSxSe1-x@ZrSiO4 Ceramic Pigments For Commercial Ink-Jet Printing. Preprint. (2021). https://doi.org/https://doi.org/10.21203/rs.3.rs-479432/v1.

[100] F. Andreola, L. Barbieri, F. Bondioli, Agricultural waste in the synthesis of coral ceramic pigment, Dyes Pigm. 94 (2012) 207–211. https://doi.org/10.1016/j.dyepig.2012.01.007.

[101] H. Gao, P. Wei, H. Liu, M. Long, H. Fu, X. Qu, Sunlight-Mediated Lead and Chromium Release from Commercial Lead Chromate Pigments in Aqueous Phase, Environ. Sci. Technol. 53 (2019) 4931–4939. https://doi.org/10.1021/acs.est.8b06839.

[102] K. Elert, M. Pérez Mendoza, C. Cardell, Direct evidence for metallic mercury causing photo-induced darkening of red cinnabar tempera paints, Commun. Chem. 4 (2021) 174. https://doi.org/10.1038/s42004-021-00610-2.

[103] E. Makarewicz, P. Cysewski, A. Michalik, D. Ziółkowska, Properties of acid or alkali treated cadmium pigments, Dyes Pigm. 96 (2013) 338–348. https://doi.org/10.1016/j.dyepig.2012.08.004.

[104] M. Hosseini-Zori, E. Taheri-Nassaj, Nano encapsulation of hematite into silica matrix as a red inclusion ceramic pigment, J. Alloys Compd. 510 (2011) 83–86. https://doi.org/10.1016/j.jallcom.2011.08.086.

[105] F. Matteucci, C.L. Neto, M. Dondi, G. Cruciani, G. Baldi, A.O. Boschi, Colour development of red perovskite pigment Y(Al, Cr)O3 in various ceramic applications, Adv. Appl. Ceram. 105 (2006) 99–106. https://doi.org/10.1179/174367606X103042.

[106] W. Hajjaji, C. Zanelli, M.P. Seabra, M. Dondi, J.A. Labrincha, Cr-doped perovskite and rutile pigments derived from industrial by-products, Chem. Eng. J. 171 (2011) 1178–1184. https://doi.org/10.1016/j.cej.2011.05.021.

[107] C. Gargori, S. Cerro, R. Galindo, A. García, M. Llusar, G. Monrós, Iron and chromium doped perovskite (CaMO 3 M = Ti, Zr) ceramic pigments, effect of mineralizer, Ceram. Int. 38 (2012) 4453–4460. https://doi.org/10.1016/j.ceramint.2012.02.019.

[108] Y. Lu, W. Dong, W. Wang, Q. Wang, A. Hui, A. Wang, A comparative study of different natural palygorskite clays for fabricating cost-efficient and eco-friendly iron red composite pigments, Appl. Clay Sci. 167 (2019) 50–59. https://doi.org/10.1016/j.clay.2018.10.008.

[109] M. Müller, J.C. Villalba, F.Q. Mariani, M. Dalpasquale, M.Z. Lemos, et al., Synthesis and characterization of iron oxide pigments through the method of the forced hydrolysis of inorganic salts, Dyes Pigm. 120 (2015) 271–278. https://doi.org/10.1016/j.dyepig.2015.04.026.

[110] J. Khanam, M.R. Hasan, B. Biswas, S.A. Jahan, N. Sharmin, et al., Development of ceramic grade red iron oxide pigment from waste iron source, Heliyon. 9 (2023) e12854. https://doi.org/10.1016/j.heliyon.2023.e12854.

[111] O. Opuchovic, A. Kareiva, Historical hematite pigment: Synthesis by an aqueous sol-gel method, characterization and application for the colouration of ceramic glazes, Ceram. Int. 41 (2015) 4504–4513. https://doi.org/10.1016/j.ceramint.2014.11.145.